Received: 22 August 2024 | Revised: 3 October 2024 | Accepted: 15 October 2024

DOI: 10.1002/app.56471

RESEARCH ARTICLE

Applied Polymer SCIENCE WILEY

PVA/AMPS hydrogels: Promising adsorbents for wastewater treatment with high efficiency and reusability

Paramjeet Yadav[1] | **Shere Afgan**[1] | **Shiwani Singh**[1] | **Ravi Prakash**[2] | **Pralay Maity**[2] | **Rajesh Kumar**[1]

[1]Department of Chemistry, Institute of Science, Banaras Hindu University, Varanasi, India

[2]School of Materials Science and Technology, Indian Institute of Technology (BHU), Varanasi, India

Correspondence
Rajesh Kumar, Department of Chemistry, Institute of Science, Banaras Hindu University, Varanasi 221005, UP, India.
Email: orajesh@bhu.ac.in

Funding information
Banaras Hindu University, Grant/Award Number: IoE 6031

Abstract

A PVAMPS hydrogel was synthesized through chemical cross-linking and semi-interpenetration of Poly (vinyl Alcohol) (PVA) and 2-Acrylamido-2-methyl-1-propanesulfonic acid (AMPS) with glutaraldehyde in distilled water. Various ratios of PVA/AMPS, namely PVAMPS-1 (2:1), PVAMPS-2 (1:1), and PVAMPS-3 (1:2), were examined to understand their individual impacts on gel formation. The synthesis of hydrogels was confirmed using FT-IR and solid-state ^{13}C NMR spectroscopy. The PVAMPS hydrogels demonstrated high efficiency as a selective adsorbent for removing cationic dyes, such as Methylene Blue, Safranine-O, and Thionine, from aqueous solutions, with over 90% removal of cationic dyes observed within 18 hours. Regeneration and reusability studies revealed that even after four cycles, the adsorption capacity of the PVAMPS hydrogels remained exceptionally high, with removal rates exceeding 90% for Methylene Blue. However, for Safranine-O and Thionine, the removal rates dropped to 20% and 23%, respectively, after four cycles. These findings underscore the promising potential of PVAMPS hydrogels for the removal of cationic dyes in wastewater treatment.

KEYWORDS

adsorption, methylene blue, safranine-O, self-healing, thionine

1 | INTRODUCTION

Synthetic dye contamination of water posed a global concern due to its adverse effects on aquatic life and human health, particularly its carcinogenic and mutagenic properties.[1] Researchers actively sought cost-effective solutions for dye removal, with adsorption being preferred for its affordability, ease of operation, and effectiveness in eliminating toxic substances.[2] This adsorption method surpassed alternative approaches like ozonation,[3] coagulation-flocculation,[4] and advanced oxidation.[5] Designing efficient adsorbents was a key focus in water remediation efforts.[6] To address this challenge, we developed a hydrogel with enhanced adsorption and desorption properties, aiming to improve dye removal efficiency.[7]

Hydrogel having a polymer network system characterized by a three-dimensional mesh structure, where water serves as the dispersed medium, and it boasts versatile physical and chemical properties that can be finely adjusted. The formation of a three-dimensional hydrogel network is facilitated by polymer chains engaging in various interactions, including covalent bonds, hydrogen bonds, physical bindings, and hydrophobic association.[8] This capability stems from the presence of multiple functional groups, such as hydroxyls, carboxyls, and amines, enabling the adsorption of dye molecules through processes such as ion exchange, chelation, van der Waals

forces, and hydrophobic interactions. The unique network structure of hydrogels allows them to swell when in contact with water without undergoing dissolution. Importantly, once the adsorption process is complete, the hydrogel can be effortlessly separated from the liquid phase.[9] Consequently, the application of hydrogels as adsorbents proves particularly well-suited for the treatment of dye pollutants in wastewater management systems. The hydrogel we synthesized here using PVA as backbone in which the hydroxyl groups of PVA backbone are bonded with the glutaraldehyde cross-linker.[10]

Polyvinyl alcohol (PVA) is a cost-effective, environmentally friendly synthetic polymer that is both biodegradable and biocompatible.[11] It is widely recognized for its ability to create superabsorbent hydrogels with excellent elasticity, chemical resistance,[12–15] and physical robustness.[16] PVA hydrogels are commonly utilized in various applications, including artificial organ implantation,[17] wound dressings,[18] drug delivery devices,[19] the textile industry,[20] and coating applications.[21] However, the use of PVA-based hydrogels in water remediation is limited due to the rigid nature of their macromolecular chains.[22] To overcome this limitation, researchers have developed modifications to PVA hydrogels.

In addition to PVA, polymers derived from 2-acrylamido-2-methyl-1-propanesulfonic acid (AMPS), commonly known as poly (AMPS) or PAMPS, have emerged as significant materials due to their remarkable water absorption capacity.[23] PAMPS is a synthetic hydrophilic polymer characterized by a strongly sulfonated group, which imparts an anionic character and high hydrophilicity to the material.[24] These polymers have found diverse applications in water purification,[25] bioengineering,[26] agriculture,[27] hygienic products,[28] food engineering,[27] and the development of electro-sensitive soft materials.[29,30] PAMPS plays a crucial role in the synthesis of different adsorbent hydrogels due to its ionizable sulfonate group, which provides exceptional chelating ability.[31] The typical synthesis process of PAMPS-based hydrogels involves free-radical polymerization of the AMPS monomer in the presence of a chemical cross-linker.[32] Despite their advantages, the mechanical properties of PAMPS-based hydrogels often fall short due to the covalently cross-linked network structure, which lacks sufficient energy dissipation.[30] Nevertheless, PAMPS has been effectively utilized for the removal of cationic dyes through electrostatic attraction between positively and negatively charged groups, highlighting the potential of PAMPS-based materials in addressing environmental and industrial challenges associated with pollutant removal and water purification.

Methylene blue (MB), a cationic dye, is widely employed in various fields such as paper, wool, and microbiology, yet its exposure can lead to health issues such as elevated heart rate and tissue necrosis.[33–36] Even brief contact with MB can result in irreversible eye damage in both humans and animals.[37] Traditional water treatment methods for effluents containing such dyes have drawbacks, emphasizing the need for efficient, cost-effective, and environmentally friendly wastewater treatment technologies, including innovative adsorbents such as agricultural waste, coffee husk-based activated carbon,[38] and natural untreated clay.[39] However, Safranin-O, a cationic versatile dye in textiles[40] and beyond, poses biodegradation challenges[41] and potential health risks, urging crucial research for its removal and environmental safety, yet its elimination through microbial means remains challenging,[42] while its exposure leads to various adverse health effects.[43] Thionine cationic dye, vital for biological staining and impacting aquatic plant photosynthesis, poses ecological threats through genetic intercalation in aquatic animals, potentially altering DNA across generations.[44]

Mahdavinia et al. modified PVA by grafting κ-carrageenan to produce κ-carrageenan/PVA nanocomposite hydrogels for the removal of crystal violet a cationic dye.[45] However, Li et al. introduced amphiphilic graphene oxide into PVA to effectively eliminate methylene blue from aqueous environments.[22] Furthermore, a functional PVA hydrogel tailored for dye removal was created by incorporating iron oxide (Fe_3O_4) nanoparticles and graphene oxides.[46] In another research article based on nanocomposite polyvinyl alcohol hydrogels reinforced with graphene-doped zinc oxide nano plates for the dye adsorption applications.[47] Moreover, in article based on Carboxymethyl chitosan/polyvinyl alcohol double network hydrogels prepared by freeze-thawing and calcium chloride cross-linking for efficient dye adsorption.[48] Another research article based on composite hydrogel which was produced by freezing–thawing treatment using chitosan, polyvinyl alcohol, and carbon black as the raw materials for the dye adsorption applications.[49]

In a prior study conducted by Omer et al., they explored the fabrication of semi-interpenetrated PVA/PAMPS hydrogel for adsorption of cationic methylene blue dye, but in our study extends this research by investigating a wider range of cationic dyes. Specifically, we assess the adsorption capabilities of Methylene blue, Safranin-O, and Thionine, each possessing distinct chemical properties. Through this comparative analysis, we aim to gain a comprehensive understanding of the hydrogel's versatility across different dye types. Additionally, our research delves into the kinetics and isotherm models governing the adsorption process for each dye, providing valuable insights into the practical applications and efficiency of the hydrogel as a reusable adsorbent material.[50]

Here, we report the hydrogel synthesis using 2-acrylamido-2-methyl-1-propanesulfonic acid (AMPS) as a monomer to modify PVA backbone. This article details the formation of hydrogels using poly (vinyl alcohol) and the cross-linking of PAMPS with a glutaraldehyde cross-linker. The synthesized PVAMPS hydrogels play a crucial role in treating water by adsorbing cationic dyes. Such as methylene blue, safranin-O, and thionine were employed to confirm the adsorption process. The confirmation was conducted using a UV–Visible spectrophotometer. The synthesis of the hydrogels was characterized through various methods, including FTIR and ^{13}CNMR, solid state NMR. The hydrogel's properties were further assessed using TGA, DSC, rheology, swelling behavior, self-healing behavior, and surface morphology analysis.

2 | EXPERIMENTAL

2.1 | Materials

Polyvinyl alcohol (PVA) polymer with a molecular weight of 160,000 g/mol and a degree of hydrolysis between 86.50 and 89.00 mol% was obtained from Himedia. The vinyl monomer AMPS (2-Acrylamido-2-methyl-1-propanesulfonic acid), dyes Safranin O (SF), Thionine (TH), Methylene blue (MB), initiator ammonium persulfate, and cross-linker glutaraldehyde were obtained from Sigma-Aldrich. Double distilled water was used throughout the experiments.

2.2 | Instrumentation

The ^{13}C NMR spectra were acquired using a JEOL AL 500 FT-NMR instrument at 20°C and a resonance frequency of 125 MHz, with DMSO-d_6 as the solvent. FT-IR spectra of all compounds were recorded using a JASCO, TOKYO-4700 spectrophotometer with ATR (attenuated total reflectance). Thermal properties of PVA, AMPS, and PVAMPS-based hydrogels were analyzed using a METTLER-TOLEDO TGA-DTA instrument under a nitrogen atmosphere. Samples were heated at a rate of 10°C/min from 30°C to 700°C. The integral procedural decomposition temperature (IPDT) was calculated by the Doyle method, and the glass transition temperature (T_g) was measured by DSC (Mettler–Toledo) at a heating rate of 10°C/min. The DSC instrument was calibrated with indium prior to use. Crystalline nature of the hydrogels was examined using XRD. Patterns were recorded on an 18 kW Cu-rotating anode Rigaku (Tokyo, Japan) instrument in the range of 10° to 80° with a scan speed of 2°/min. SEM images of hydrogels with and without adsorption were obtained using a Carl Zeiss-Evo-18 research model (Germany) after Au coating. Dye adsorption studies were performed using a Carry 60 UV–Vis Agilent-USA spectrophotometer. Surface area and pore diameter analysis of the synthesized hydrogels were determined using an Autosorb (IQ2) instrument from Quantachrome Instruments (USA). Viscoelastic studies were carried out on a Malvern instrument Limited, UK (model: Bohlin Gemini 2), equipped with 25 mm parallel plates and a 500-micron gap.

2.3 | Methods

2.3.1 | Synthesis of PVAMPS hydrogel

The synthesis of PVAMPS hydrogels with different PVA/AMPS ratios (2:1, 1:1, and 0.5:1) was provided in Table 1. To create the hydrogels, 2 g of PVA was dissolved in 100 mL of distilled water until a clear solution was achieved. Following that, 2 g of AMPS was added to the solution, and the mixture was stirred for an hour until it became a clear solution. An initiator, ammonium per sulphate, was then added, and the reaction mixture was allowed to initiate for 10 min. Glutaraldehyde cross-linker was subsequently added to the reaction mixture, and the mixture was stirred for 15 min until it became viscous and eventually formed into a hydrogel (Figures 1 and 2). The entire reaction process was conducted in atmospheric conditions.

In this study, PVAMPS hydrogel was synthesized through the cross-linking of poly (vinyl alcohol) (PVA) chains, forming a cage-like structure. This structure was subsequently embedded with a semi-interpenetrating network of poly (AMPS). The hydrogen of poly (AMPS)

TABLE 1 Different ratio of backbone (polyvinyl alcohol) and APMS in mol/L during synthesis of PVAMPS hydrogels.

Sr. no.	PVA mol/L	Monomer AMPS (mol/L)	Cross-linker glutaraldehyde (in µL)	Initiator ammonium persulphate (mol/L)	Time of gelation (min)
1.	1.25×10^{-4}	2.41	30	0.001	25
2.	0.62×10^{-4}	3.62	30	0.001	45
3.	0.31×10^{-4}	4.82	30	0.001	60

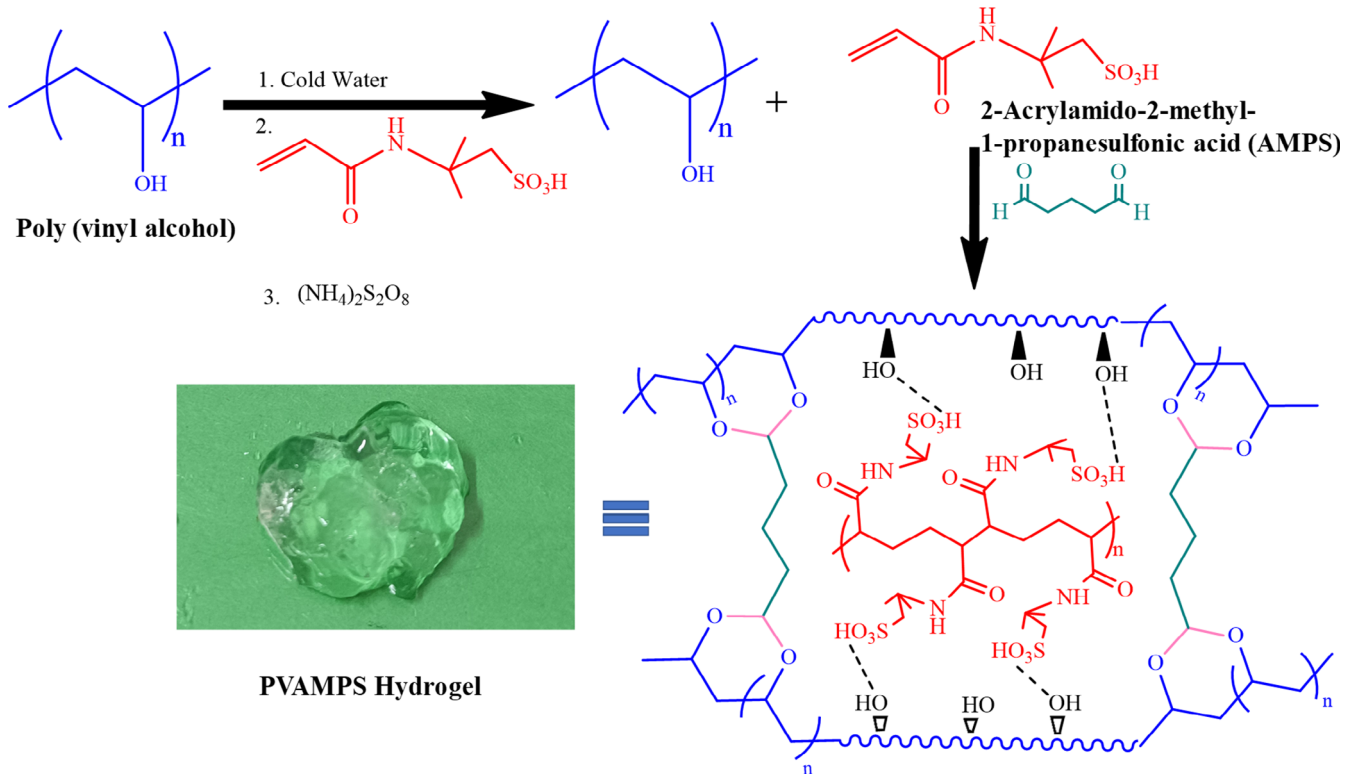

FIGURE 1 Synthesis of PVATU hydrogels represented by chemical reaction. [Color figure can be viewed at wileyonlinelibrary.com]

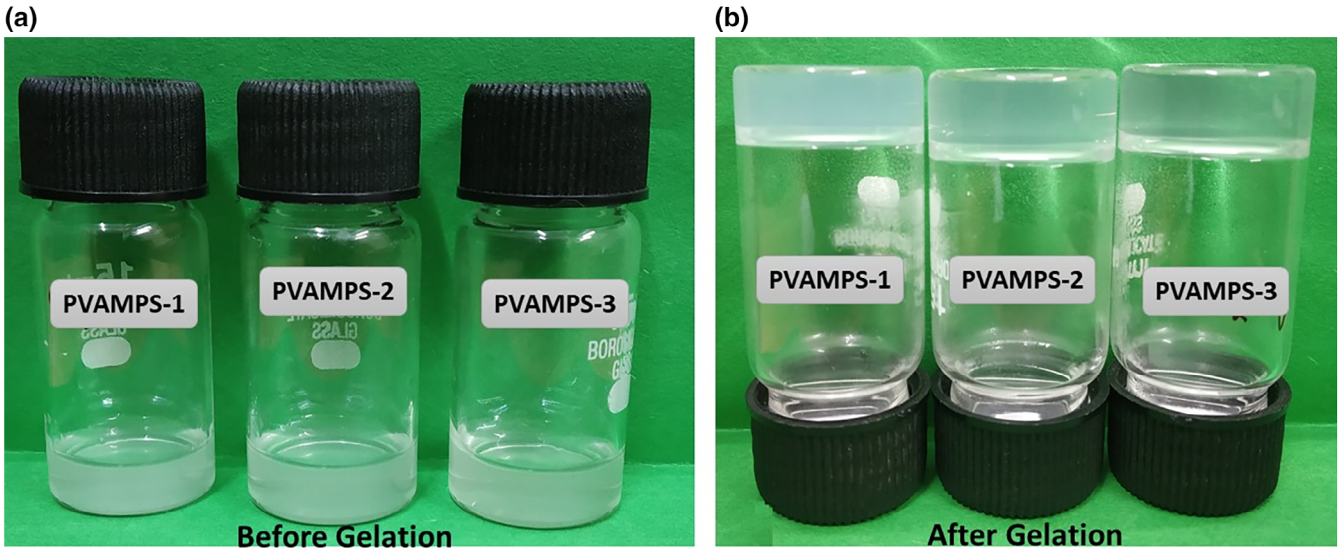

FIGURE 2 Confirmation of synthesis of PVAMPS-1, PVAMPS-2 and PVAMPS-3 hydrogels, (a) Before gelation PVAMPS in solution form, (b) After gelation thick gelation properties of PVAMPS hydrogels. [Color figure can be viewed at wileyonlinelibrary.com]

interact with the oxygen atoms of PVA via hydrogen bonding, resulting in the formation of the PVAMPS hydrogel. To examine the impact of different component ratios, varying concentrations of PVA and poly (AMPS) were tested, with the results confirmed through FTIR and solid-state NMR analysis.[51]

2.3.2 | Rheology study

Rheometry is a powerful tool for studying the curing of thermoplastic polymer and for the estimation of visco-elastic materials functions such as dynamic shear moduli, for example, storage modulus (G') (Equation 1) and loss

modulus (G'') (Equation 2).[52] The rheological behaviors of PVAMPS Hydrogels were determined using Anton Paar MCR 702 (multi-drive) rheometers using the parallel-plate geometry (diameter 25 mm) at room temperature and the gap between these plates was kept 1 mm fixed during the measurements. The viscoelastic properties of each of the PVAMPS Hydrogels were estimated by linear viscoelastic region (LVER) applying constant strain. The complex viscosity, loss modulus and frequency sweep measurement with angular frequencies range (ω) range of 0.1–100 rad/s (Figure 9a). The storage modulus (G') is defined following equation, which is the amplitude ratio of the component of the stress (σ_0) in phase with the strain to the strain amplitude (γ^0):

$$G' = \frac{\sigma_0 \cos(\delta)}{\gamma^0} \quad (1)$$

where, δ phase angle between stress and stress.

Similarly, the loss modulus (G'') is the amplitude ratio of the component of the stress in quadrature with strain to the strain amplitude:

$$G'' = \frac{\sigma_0 \sin(\delta)}{\gamma^0} \quad (2)$$

For the perfect solid, the strain and stress waveforms are in the phase with $\delta = 0°$ G' are having the finite value but G'' becomes zero. If the frequency oscillation was applied on the materials at a given value of γ^0, the energy stored elastically by the system per cycle was measured through G' and also for the perfect liquid, the stress and strain waveforms are in quadrature, that is, $\delta = 90°$ and G'' has finite value, whereas G' becomes zero. Hence, in this situation, the energy that is dissipated during flow per cycle of frequency oscillation for a finite value of shear rate ($\dot{\gamma}$) is measured through G''. The frequency sweep measurement was performed at 30°C for hydrogel (Figure 9b,c).[53]

The viscosity flow curve of the prepared PVAMPS Hydrogels was measured by a multi-drive MCR 702 Anton Paar rheometer with parallel geometry with 25 mm and the gap between this plates was set 1 mm constant for each measurement. The viscosity flow curve is measured as a function of shear rate ($\dot{\gamma}$) with a range of 0.1–100 s^{-1} for the PVAMPS Hydrogels (Figure 9d).[54]

The steady shear measurement gives the viscosity of the materials with respect to time (viscosity is the function of time) at a constant shear rate ($\dot{\gamma}$). The viscosity of the PVAMPS Hydrogels was measured by applying the steady shear test using the Anton Paar MCR 702 (multi-drive) rheometer with the parallel-plate geometry (diameter 25 mm) at a constant shear rate (Figure 9e,f).[55]

2.4 | Surface morphology study

To conduct SEM analysis, it is crucial to ensure the sample is entirely dry and absence of impurities. The surface can be purified by either using methanol solvent or blowing pressurized air to eliminate any debris particles. After cleaning, the samples were washed with water, dried, and affixed to double-sided taped metal stubs before coating them with gold for SEM examination (Figure 10a–f).[56]

2.5 | Thermal behavior study

TGA analysis was performed to determine the thermal stability of chemically modified PVAMPS hydrogels with AMPS and PVA. For this, approximately 4–6 mg of PVA, AMPS, and PVAMPS hydrogels were heated from room temperature to 600°C at a heating rate of 10°C/min under nitrogen (Figure 11a,b)[57] and graph of weight loss plotted against the time/ temperature.

2.6 | Determination of glass transition temperature

To ascertain the crystallization/melting temperature of the sample, the water content was eliminated by placing it in a desiccator containing silica gel. The DSC instrument was calibrated utilizing Indium, and 4 mg of the average sample amount was employed for analysis. The intersection points of the two tangents of the transition peak determined the crystallization/melting temperature (Figure 11c).[58]

2.7 | Study of crystalline/amorphous nature

The crystalline/amorphous properties of AMPS, PVA, and synthesized PVAMPS hydrogels were analyzed using the Bruker D8 Advance (Eco) instrument for powder X-ray diffraction analysis. A copper tube with a λ value of 1.5418 Å and a 2θ range of 10° to 80° against intensity was employed to examine the samples. The scanning speed was set to 2°/min, and the outcomes are shown in Figure 12.[59]

2.8 | Self-healing behavior: physical and rheological experiment

To evaluate the self-healing ability of PVAMPS hydrogels, two slices were sliced with a sharp blade and positioned adjacent to each other on a flat glass dish (Figure 3a–g).

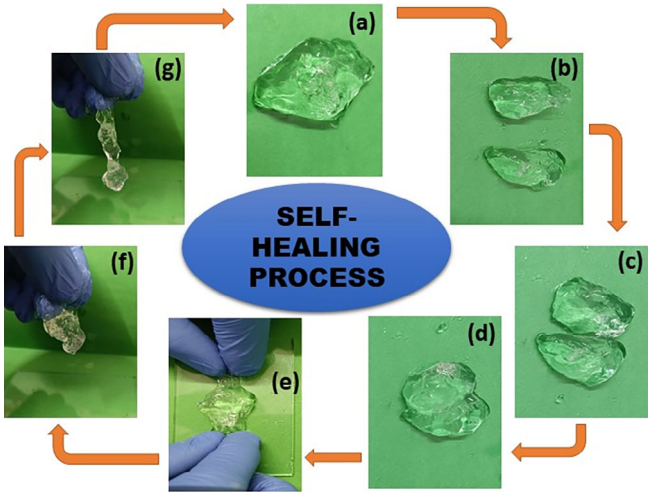

FIGURE 3 Image shows that the confirmation of the self-healing behavior of PVAMPS hydrogel is demonstrated by physical experimentation: (a) image of PVAMPS hydrogel, (b) after cutting PVAMPS hydrogel apart in two parts, (c) this image indicates the PVAMPS hydrogel ready for self-healing, (d–g) in this image self-healing is confirmed with different type of stretching. [Color figure can be viewed at wileyonlinelibrary.com]

The process was photographed at various time points. Without any external stimuli, the two parts of the PVAMPS hydrogels were observed to have healed after 30 min at room temperature.[60]

2.9 | Water absorption study

To explore the water retention ability of PVAMPS hydrogels, the swelling study (Figure 4) was carried out in water. Initially, the PVAMPS hydrogels were dehydrated in a vacuum until they attained a constant weight, then soaked it in distilled water at 37 ± 0.1°C and allowed it to expand in water at various pH levels (4, 7 and 9). At different time intervals, the swollen hydrogels were removed from the medium and weighed until they achieved equilibrium. Using Equation (3)[61,62] determined the quantity of water present in the PVAMPS hydrogels.

$$\text{Degree of swelling of hydrogels} = \frac{W_s - W_o}{W_o} \times 100 \quad (3)$$

where W_s, wt. of swollen PVAMPS hydrogels, W_o, the original wt. of the PVAMPS hydrogels.

2.10 | BET (Brunauer–Emmett–teller) analysis

The surface area and average pore size of the hydrogels were determined using the Barrett–Joyner–Halenda (BJH) method. Nitrogen adsorption/desorption was assessed at 77.4 K through volumetric gas adsorption studies employing a Brunauer–Emmett–Teller (BET) surface analyzer (Quantachrome Instruments, USA, Model-Autosorb IQ2) within a pressure range of 0–900 mmHg. Before the measurements, the samples underwent overnight degassing at 150°C to eliminate any gases, particularly bound moisture, adhering from the atmosphere (Figure 14).[63]

2.11 | Dye adsorption and removal study

Dye adsorption experiments were performed on the different combination having PVAMPS hydrogels by combining 10 mg of the hydrogel with dye solutions containing Methylene blue, Safranine-O, and Thionine at different concentrations of 5, 10, 20, 30, 40, and 50 ppm. The mixture was placed in a covered glass vial at room temperature. To monitor the change in dye concentrations, a 500 μL of supernatant was consistently withdrawn from the mixture at specified time intervals (i.e., from 60 to 2160 min). The collected supernatants were then diluted with 3 mL of water, and then filtered using the 0.22-μm nylon membrane syringe filter (Figure 5). They were then analyzed by the UV–visible spectrophotometer (Figure 6). All the samples removed at different time intervals were examined and compared with the initial sample without any adsorbent to determine the amount of dye removed and the effect of the contact time and the maximum absorbance was measured to determine the adsorbed amounts of the dyes.

Following the adsorption process, the hydrogel was extracted from the water solution, transferred to a 50 mL neutral solution at 298 K, incubated for 12 h, and washed with 30 mL of water (3 times, 30 min each). After drying at 75°C, the recovered PVAMPS hydrogel was prepared for the next cycle of desorption. This adsorption–desorption procedure was repeated seven times. The adsorption capacity of PVAMPS hydrogels for MB, SF and TH at adsorption time Q_t and equilibrium time Q_e were calculated using Equations (4) and (5), respectively.[64,65] Removal efficiency (RE) of MB, SF and TH was determined using Equation (6).[66]

$$Q_t = \frac{(C_0 - C_t)V}{m} \quad (4)$$

$$Q_e = \frac{(C_0 - C_e)V}{m} \quad (5)$$

$$\%\text{RE} = \frac{C_0 - C_e}{C_0} \times 100\% \quad (6)$$

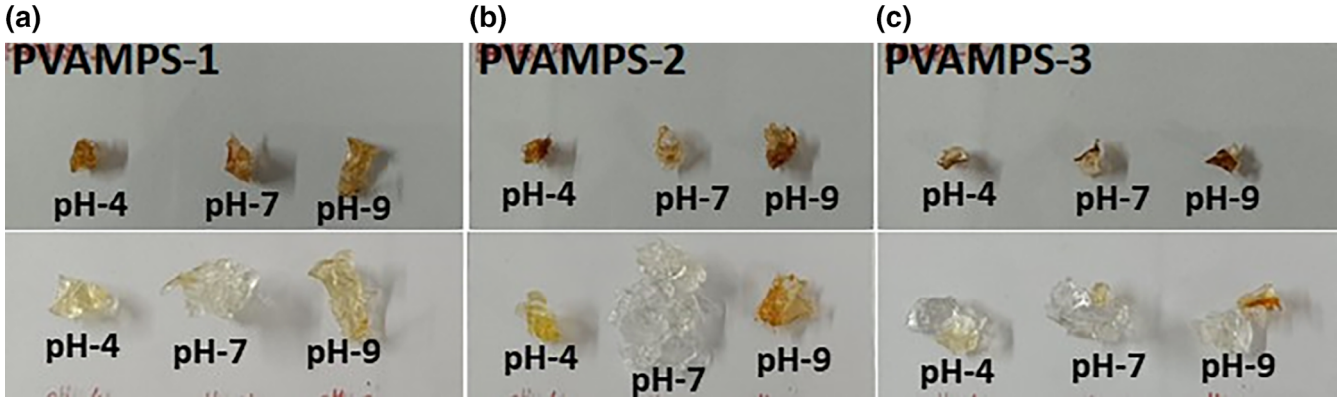

FIGURE 4 Observation of swelling behavior of PVAMPS-1, PVAMPS-2 and PVAMPS-3 at different pH (4.0, 7.0 and 9.0), (a) swelling behavior of PVAMPS-1 (1.25×10^{-4} mol/L of poly (vinyl alcohol) and 2.41 mol/L of AMPS) at different pH is shown, (b) swelling behavior of PVAMPS-2 (0.62×10^{-4} mol/L of poly (vinyl alcohol) and 3.62 mol/L of AMPS) at different pH is shown and (c) swelling behavior of PVAMPS-3 (0.31×10^{-4} mol/L of poly (vinyl alcohol) and 4.82 mol/L of AMPS) at different pH is shown. [Color figure can be viewed at wileyonlinelibrary.com]

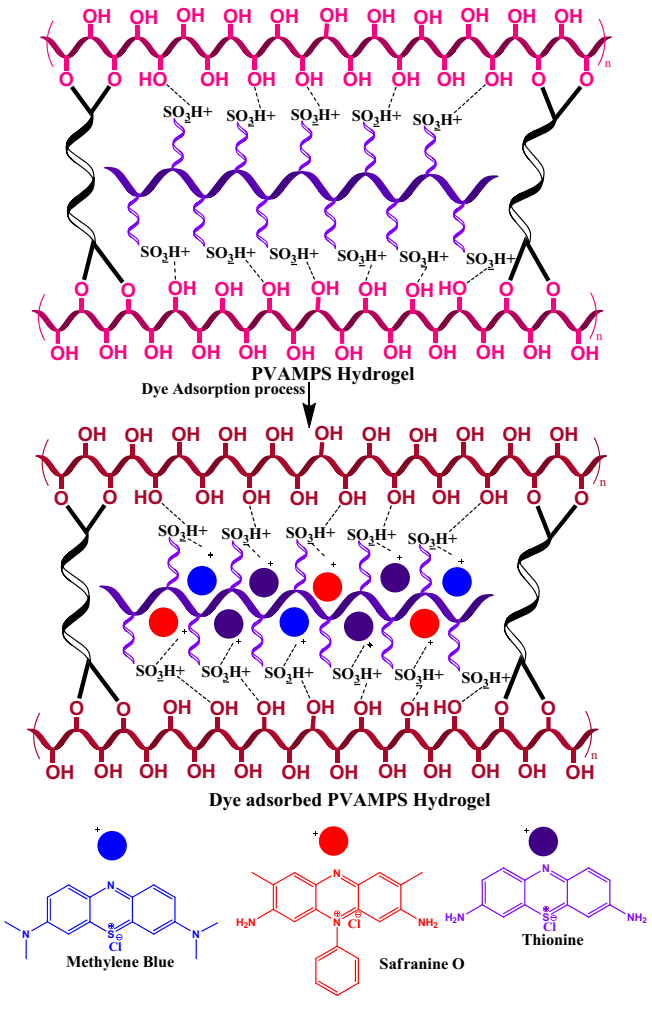

FIGURE 5 In this presentation of reaction is shows that type of attractions between PVAMPS hydrogels and dyes (i.e. MB, SF and TH) towards synthesized PVAMPS hydrogels. [Color figure can be viewed at wileyonlinelibrary.com]

3 | RESULTS AND DISCUSSION

3.1 | FTIR analyses of PVAMPS hydrogel

Figure 7 shows the FTIR spectra of PVA, AMPS, and PVAMPS hydrogels. In AMPS spectrum, the absorption band at 1607 cm^{-1}, corresponding to the C=C bond, vanished after gelation. The AMPS spectrum exhibited a distinctive absorption peak at 3300 cm^{-1} attributable to the N–H group vibration. Additionally, peaks at 2941 and 2854 cm^{-1} associated with the C-H stretching frequencies of $-CH_3$ and $-CH_2$ groups were observed. The absorption band at 1407 cm^{-1} was attributed to the C=O vibration, and peaks at 1102 and 1009 cm^{-1} were related to the S–O vibration in the sulfonic group.[67]

Conversely, the PVA spectrum revealed bands at 3459, 2920, and 1214 cm^{-1} corresponding to the stretching of the O–H, C–H, and C–O groups, respectively.[68] In the PVAMPS hydrogels spectra, observed between 1608 and 1627 cm^{-1} were evident for the presence of C=O group. Furthermore, the broad absorption band at 3459 cm^{-1} in PVA, associated with OH groups, shifted to a higher wavenumber (3437 cm^{-1}) in the PVA/PAMPS hydrogel, with a decrease in intensity. The stretching vibration of C-H at 2920 cm^{-1} in the PVA spectrum also shifted to 2929 cm^{-1} in the PVA/PAMPS spectra. Additionally, the C-O band at 1043 cm^{-1} in PVA was replaced by broader absorption bands at 1118 and 1036 cm^{-1} in the PVA/PAMPS hydrogel. The bands 1118 and 1036 cm^{-1} were attributed to SO_3^- and O=S=O stretching in SO_3H groups, suggesting the presence of AMPS. The peak at 927 cm^{-1} in the PVAMPS hydrogel confirmed the existence of a C–O–C bond between –OH in PVA and –CHO in GA,[69] affirming successful chemical cross-linking (Figure 7).

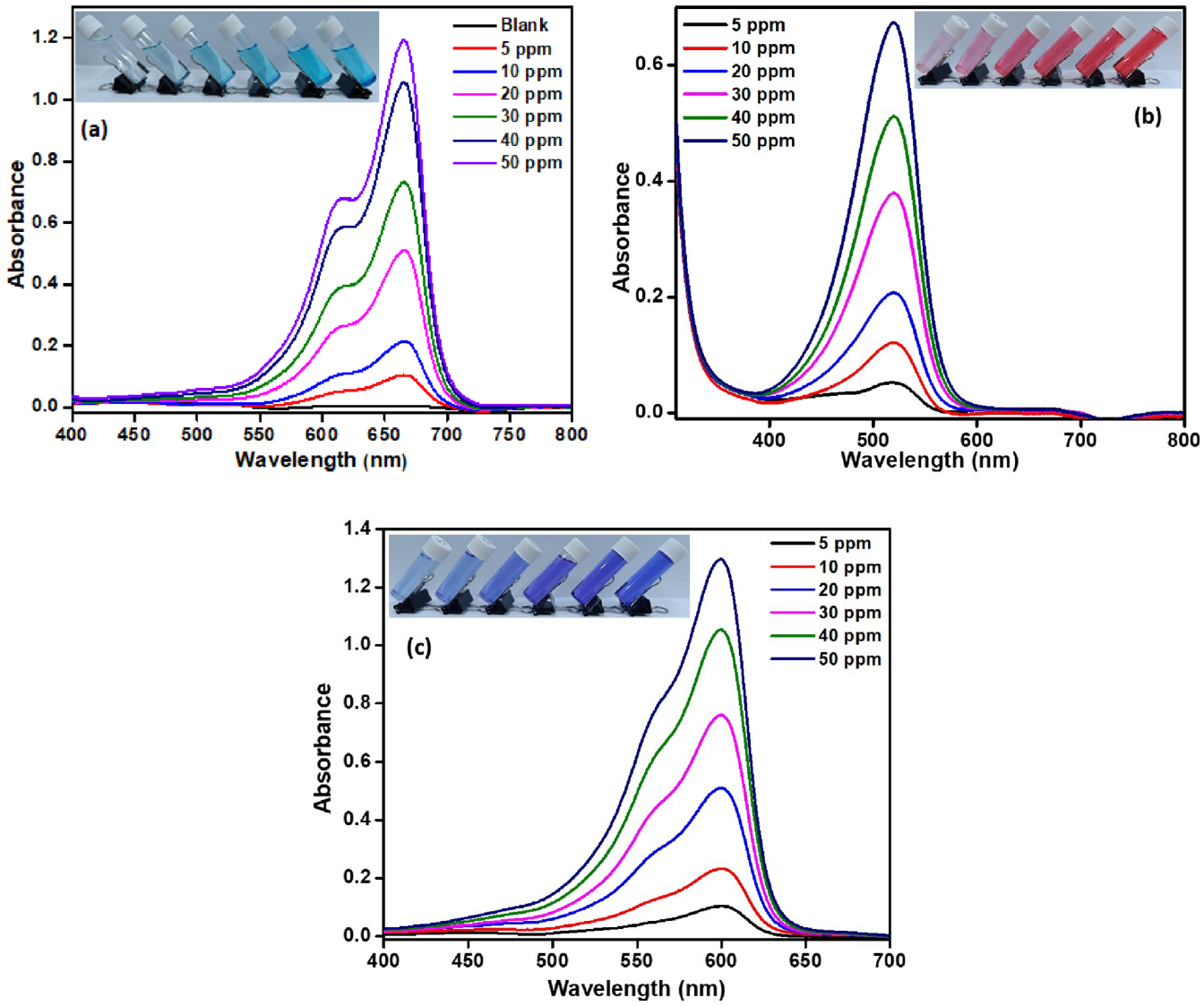

FIGURE 6 This image shows that the wavelength of solutions of dye for different concentration (i.e. 5, 10, 20, 30, 40 and 50 ppm) of MB, SF and TH dyes. (a) UV–visible spectra for MB dye solutions. (b) UV–visible spectra for SF dye solutions. (c) UV–visible spectra for TH dye solutions. [Color figure can be viewed at wileyonlinelibrary.com]

The Poly (vinyl alcohol) structure was analyzed using ^{13}C NMR in DMSO-d_6 (Figure 8). The chemical shift values at 41 ppm and 80 ppm substantiate the presence of $-CH_2$ (b) and –CH (a) groups, respectively.[70] For 2-Acrylamido-2-methyl-1-propanesulfonic acid (AMPS), ^{13}C NMR in DMSO-d_6 revealed chemical shift values at 26 ppm ($-CH_3$) (g), 51 ppm (–C) (f), 60 ppm ($-CH_2$) (h), 124 ppm = CH_2 (c), 134 ppm (=CH) (d), and 165 ppm (–C=O) (e).[71] The structure establishment of the PVAMPS hydrogel was achieved through ^{13}C CP-TOSS solid-state NMR due to the hydrogel's solubility problem. New chemical shift values at 25 ppm (–CH–CO–) and ($-CH_2-$) (m and n), 54 ppm ($-CH_2$) (j and k), and 65 ppm (–O–CH–O) (i) were observed. In comparison with poly (vinyl alcohol) and AMPS, cross-linked bonds were attached on both sides of Glutaraldehyde with -OH of poly (vinyl alcohol) and poly AMPS.[72] The emergence of new peaks affirms the formation of the cross-linked PVAMPS hydrogel.

3.2 | Mechanical strength of PVAMPS hydrogels

3.2.1 | The effect of chemical cross-linking on rheological behavior

Rheological measurements offer insights into the micro-structural changes occurring within PVAMPS hydrogels and their distinct behavior compared to physical mixtures

and interpenetrating behavior of poly AMPS, depending on the interaction between the backbone and polymer across varying angular frequencies. Figure 9a–c depict measurements of storage modulus, loss modulus, and complex viscosity for the hydrogels. The storage moduli exhibit an almost parallel relationship with increasing frequency for all samples, indicating the three-dimensional network nature of PVAMPS hydrogels and PVA hydrogel (Figure 9a). The presence of a cross-linker and interpenetrating behavior of poly AMPS enhances hydrogel strength, with PVAMPS-2 showing the highest modulus (i.e., G' is 1355 Pa and G'' is 37 Pa) due to chemical cross-linking with the polymer chain of poly (vinyl alcohol) and interpenetration of AMPS in compression of the PVA hydrogel composed solely of poly (vinyl alcohol). The loss moduli gradually increase with frequency for all PVAMPS hydrogels, with PVAMPS-2 displaying the highest relative value of loss modulus (i.e., 224 Pa). In typical hydrogels, the storage moduli are higher than the loss moduli. This characteristic is observed in all PVAMPS and PVA hydrogels. The complex viscosity decreases gradually with increasing frequency for all three PVAMPS and PVA hydrogels, and PVAMPS-2 exhibits the highest viscosity (i.e., 1.35×10^7 mPa) due to the chemical connectivity of poly (vinyl alcohol) and interpenetration of poly AMPS.[73] However, the viscosity of poly AMPS in the presence of glutaraldehyde surpasses that of the PVA hydrogel, attributed to changes in the microenvironment and the absence of interpenetration of poly AMPS with poly (vinyl alcohol) hydrogels.

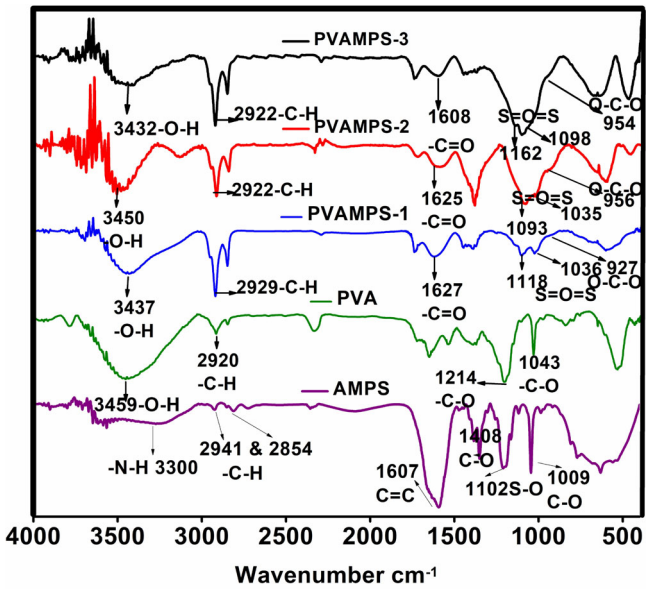

FIGURE 7 IR spectrum of monomer and hydrogels: PVA, AMPS, PVAMPS-1 (1.25×10^{-4} mol/L of poly (vinyl alcohol) and 2.41 mol/L of AMPS), PVAMPS-2 (0.62×10^{-4} mol/L of poly (vinyl alcohol) and 3.62 mol/L of AMPS) and PVAMPS-2 (0.31×10^{-4} mol/L of poly (vinyl alcohol) and 4.82 mol/L of AMPS) is mentioned, which confirms the presence of functionality of AMPS and PVA and also it confirms the formation of PVAMPS -1, PVAMPS -2 and PVAMPS -3 Hydrogels. [Color figure can be viewed at wileyonlinelibrary.com]

3.2.2 | Viscous flow behavior

In Figure 9d, the flow behavior of PVAMPS-1, PVAMPS-2, PVAMPS-3, and the PVA hydrogels at 30°C is shown across a broad range of shear rates. The PVA hydrogel demonstrates lower shear viscosity (i.e., 1.38×10^5 mPa)

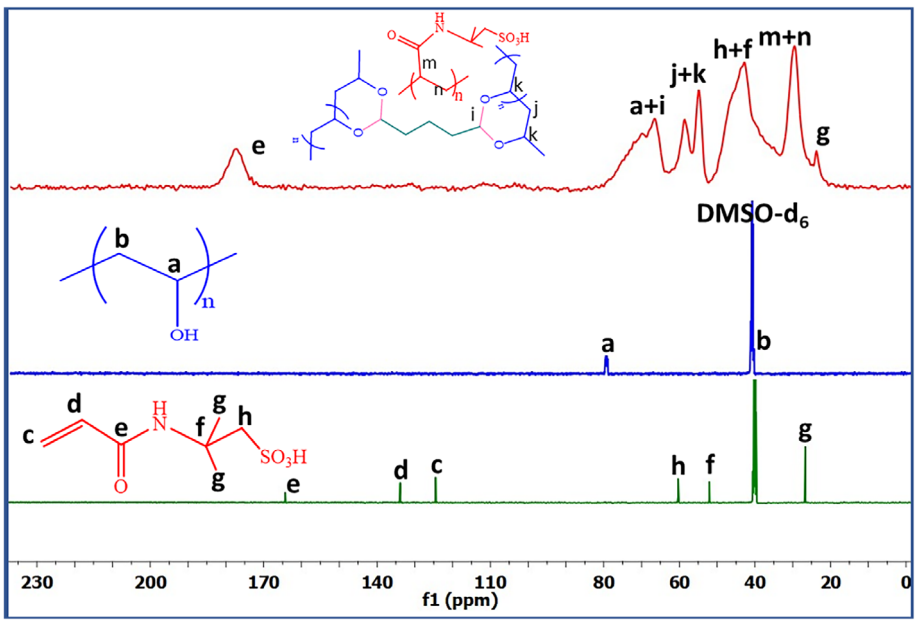

FIGURE 8 ^{13}C NMR spectrum of polymer (PVA), monomer (AMPS), and ^{13}C Solid NMR spectrum of hydrogels: PVA, AMPS, PVAMPS-1 (1.25×10^{-4} mol/L of poly (vinyl alcohol) and 2.41 mol/L of AMPS), PVAMPS-2 (0.62×10^{-4} mol/L of poly (vinyl alcohol) and 3.62 mol/L of AMPS) and PVAMPS-2 (0.31×10^{-4} mol/L of poly (vinyl alcohol) and 4.82 mol/L of AMPS) is mentioned, which confirms the presence of functionality of AMPS and PVA and also it confirms the formation of PVAMPS -1, PVAMPS -2 and PVAMPS -3 Hydrogels. [Color figure can be viewed at wileyonlinelibrary.com]

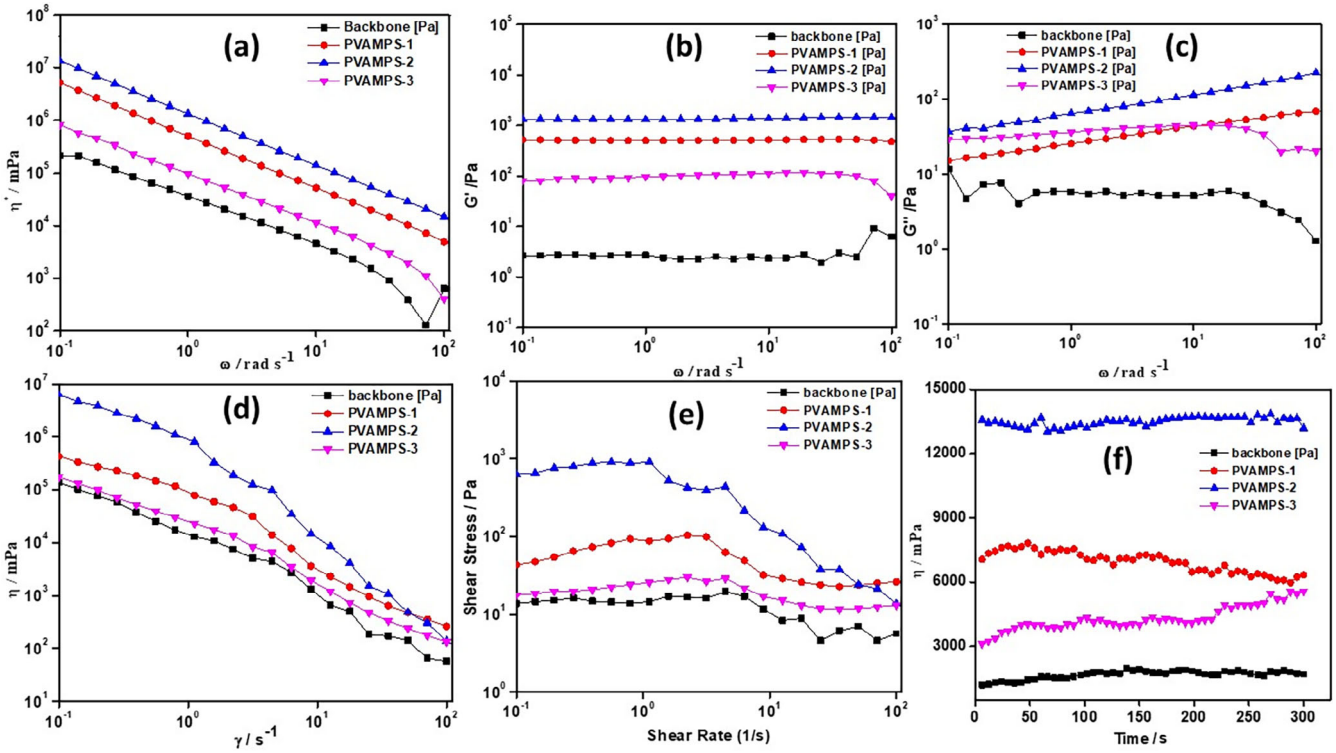

FIGURE 9 Rheological behavior of PVAMPS-1 (1.25×10^{-4} mol/L of poly (vinyl alcohol) and 2.41 mol/L of AMPS), PVAMPS-2 (0.62×10^{-4} mol/L of poly (vinyl alcohol) and 3.62 mol/L of AMPS) and PVAMPS-3 (0.31×10^{-4} mol/L of poly (vinyl alcohol) and 4.82 mol/L of AMPS) hydrogels and Poly (vinyl alcohol) (Precursor) on the behalf of storage modulus (G') and loss modulus (G'') different parameters, (a) complex viscosity as a function of angular frequency measured at 30°C is mentioned in this plot, (b) Frequency sweep measurement of polymer PVAMPS hydrogels in terms of storage modulus as a function of angular frequency measured at 30°C is mentioned in this plot, (c) Frequency sweep measurement of PVAMPS hydrogels in terms of loss modulus as a function of angular frequency measured at 30°C is mentioned in this plot, (d) viscosity flow curve behavior of PVAMPS-1, PVAMPS-2 and PVAMPS-3 as a function of shear rate; (e) Shear Stress measurement of PVAMPS-1, PVAMPS-2 and PVAMPS-3 as function of shear rate. (f) Constant shear measurement of PVAMPS hydrogels as a function of time. [Color figure can be viewed at wileyonlinelibrary.com]

and less viscous (i.e., 2.15×10^5 mPa) behavior, while all three PVAMPS-1, PVAMPS-2, and PVAMPS-3 hydrogels exhibited a continuous decrease in viscosity which is 4.3×10^5 mPa to 2.6×10^2 mPa, 6.37×10^6 mPa to 1.3×10^2 mPa and 1.7×10^5 mPa to 1.3×10^2 mPa respectively. It is noteworthy that chemically cross-linked and interpenetrating PVAMPS-1, PVAMPS-2, and PVAMPS-3 hydrogels consistently display significantly higher viscosity compared with the physical mixture across the entire range of shear rates studied. The PVA hydrogel displays shear-thinning behavior with a less pronounced Newtonian plateau, indicative of a weak hydrogel with reduced viscous characteristics.[73] In contrast, the Newtonian plateau diminishes for PVAMPS-1, PVAMPS-2, and PVAMPS-3 hydrogels due to the presence of a cross-linker (glutaraldehyde) and the interpenetration of poly AMPS in the physical mixture (PVAMPS-2). Substantial shear thinning is observed in PVAMPS-1 and PVAMPS-3 hydrogels due to non-ideal behavior resulting from the chemical cross-linking of glutaraldehyde with poly (vinyl alcohol) and the interpenetration of the poly AMPS chain.

Consequently, the chemical cross-linking of glutaraldehyde and interpenetration in the polymer matrix enhances the viscosity of PVAMPS hydrogels compared to the PVA hydrogel. In Figure 9f, the steady shear viscosity over time is presented for all three hydrogels (PVAMPS-1, PVAMPS-2, PVAMPS-3, and the blank hydrogel) at a shear rate of $\dot{\gamma} = 1\,s^{-1}$. The initial viscosity values for PVAMPS-1, PVAMPS-2, PVAMPS-3, and the blank hydrogels are 7065, 13,574, 3120, and 1193 mPa, respectively. A slight reduction in viscosity is observed over a longer time scale for the PVA hydrogel, attributable to its weak nature and may be due to the absence of interpenetrating behavior causing a disordered structure under the shearing effect (Figure 9e,f). The viscosity of the synthesized PVAMPS hydrogels increases proportionally with the concentration of poly (vinyl alcohol) and poly AMPS, cross-linked with glutaraldehyde, leading to the interpenetration of poly AMPS and the formation of

hydrogels. Notably, the absolute value of the steady shear viscosity of PVAMPS-2 is significantly higher (i.e., 637 Pa) than that of PVAMPS-1 (i.e., 44 Pa), PVAMPS-3 (i.e., 18 Pa), and the PVA (i.e., 14 Pa) hydrogels, indicating a more pronounced cross-linking and interpenetrating effect in the PVAMPS-2 hydrogel.

3.3 | Morphological study (scanning electron microscopy)

SEM was employed to assess the surface morphology of PVAMPS hydrogels pre- and post-dye adsorption. Unlike PVAMPS, which exhibits a coarse fiber-like structure, PVA displays a sleek, dense, and uniform appearance (Figure 10b), while AMPS exhibits a crystalline nature (Figure 10a). The rough surface of PVAMPS is likely a result of Glutaraldehyde cross-linking with the alcoholic -OH groups of PVA, altering its properties. Furthermore, SEM images of various PVAMPS compositions (Figure 10c–e) were captured at different PVA and AMPS ratios (i.e. PVAMPS-1 (1.25×10^{-4} mol/L of poly (vinyl alcohol) and 2.41 mol/L of AMPS), PVAMPS-2 (0.62×10^{-4} mol/L of poly (vinyl alcohol) and 3.62 mol/L of AMPS) and PVAMPS-3 (0.31×10^{-4} mol/L of poly (vinyl alcohol) and 4.82 mol/L of AMPS)), which further confirms the formation of distinct fibrils in PVAMPS connected during gelation. Additionally, Figure 10f–h illustrate dye adsorption on the surface of PVAMPS hydrogels, manifested as small particles clearly visible in SEM images, thereby confirming the effectiveness of PVAMPS hydrogels in dye adsorption.

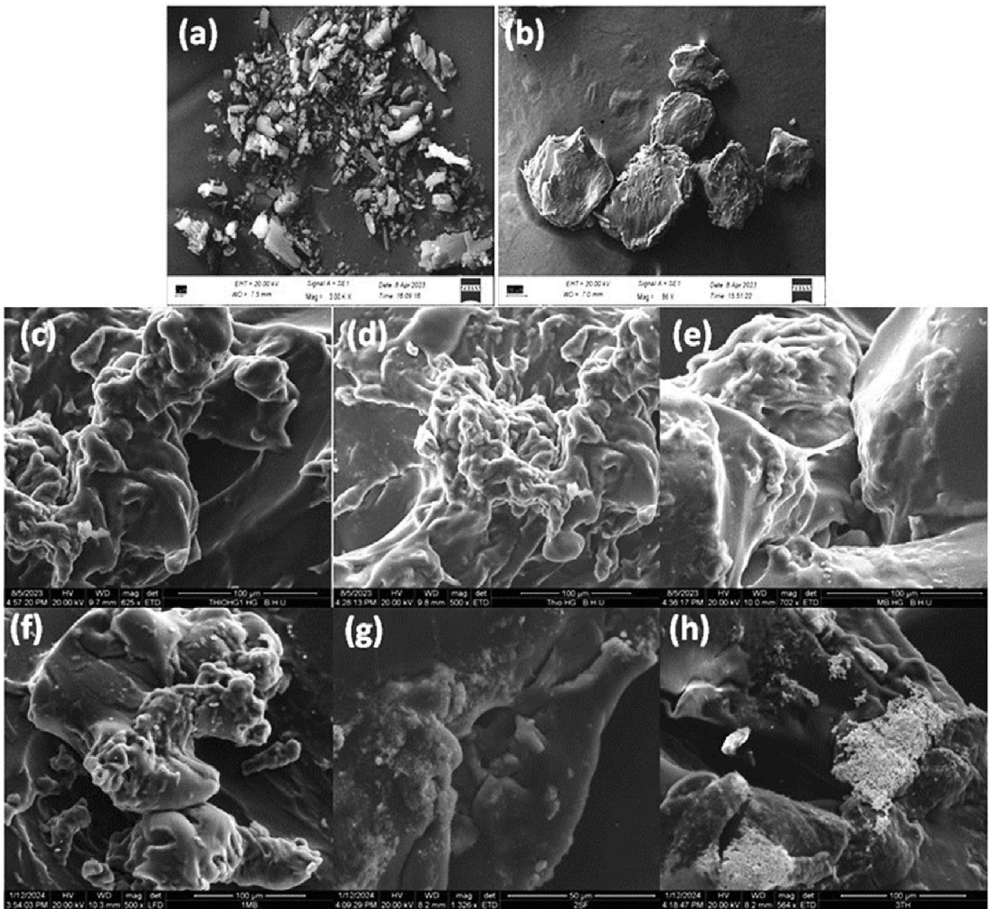

FIGURE 10 In the above Images confirmation of morphology of AMPS, PVA, PVAMPS-1, PVAMPS-2 and PVAMPS-3 with the help of Scanning Electron Microscope (a) provides information about the crystalline nature of AMPS (b) confirms the amorphous nature of PVA (Backbone) (c) confirms the porous nature of PVAMPS-1 (1.25×10^{-4} mol/L of poly (vinyl alcohol) and 2.41 mol/L of AMPS) (d) porosity of PVAMPS-2 (0.62×10^{-4} mol/L of poly (vinyl alcohol) and 3.62 mol/L of AMPS) slight decreases due to the variation of the ratio of AMPS and PVA (e) the crystallinity is observed in PVAMPS-3 (0.31×10^{-4} mol/L of poly (vinyl alcohol) and 4.82 mol/L of AMPS) due to the variation of the ratio of AMPS and PVA (f) shows the adsorption of dye on the surface of PVAMPS-1 (1.25×10^{-4} mol/L of poly (vinyl alcohol) & 2.41 mol/L of AMPS) (g) shows the adsorption of dye on the surface of PVAMPS-2 (0.62×10^{-4} mol/L of poly (vinyl alcohol) & 3.62 mol/L of AMPS) slight decreases due to the variation of the ratio of AMPS and PVA (h) shows the adsorption of dye on the surface PVAMPS-3 (0.31×10^{-4} mol/L of poly (vinyl alcohol) & 4.82 mol/L of AMPS) due to the variation of the ratio of AMPS and PVA.

3.4 | TGA studies

Figure 11a,b shows the thermal stability and degradation characteristics of the PVAMPS hydrogel matrix. Notably, AMPS degradation unfolds in two distinct stages. Interestingly, both PVA and AMPS exhibit a single weight loss of around 2% below 100°C. This phenomenon can likely be attributed to the hydrophilic nature of both materials, leading to strong water molecule interactions within the PVA backbone and AMPS itself, resulting in moisture loss at low temperatures.[74]

Anhydrous complexes form during the early stages of thermal degradation due to water molecule removal. PVAMPS hydrogels, unlike PVAMPS itself, undergo three distinct degradation steps during thermal analysis. For AMPS degradation, the first stage occurs between 176–213°C, resulting in a 29% mass loss (Tables S1 and S2, Figure 11a,b), which is also observed in DTA as an exothermic peak at 110°C, likely involves the loss of water molecules present as moisture. The second stage, between 218–345°C, results in a 40% mass loss at 235°C, likely due to the degradation of the amide group in poly AMPS. PVA degradation, the first stage for PVA occurs between 221–416°C (Tables S1 and S2, Figure 11a,b) with a 36% mass loss. This likely involves the degradation of the side-chain hydroxyl (O–H) groups of PVA at 329°C. The second stage, at 416–497°C, shows a 79% mass loss at 431°C, likely due to the cleavage of the C–C backbone of the PVA polymer. PVAMPS hydrogels degradation, despite different poly (vinyl alcohol) to poly AMPS ratios, the TG curves of all three PVAMPS hydrogels share some similarities, The first stage (112–232°C) leads to a 14%–15% weight loss for PVAMPS-1 and -2, and 13% for PVAMPS-3, likely due to moisture loss. The second stage (235–355°C) results in a 46–48% weight loss for all three hydrogels, likely due to AMPS amide group degradation. The third stage (365–521°C) causes a 64%–66% weight loss at 338–339°C, possibly due to the breakdown of interpenetrating interactions between poly AMPS and the hydrogel network. Introducing AMPS into the hydrogels reduces their thermal stability compared to pure PVA. This is evident from the lower decomposition temperatures and higher mass losses observed for PVAMPS hydrogels at all stages of thermal degradation.

3.5 | DSC studies

The high-temperature stability of PVAMPS hydrogels was confirmed using TGA up to ~460°C. To further understand their phase transition behavior at room temperature relevant to wastewater treatment applications, we performed DSC analysis.[75] Figure 11c presents the DSC thermograms of PVA, AMPS, and PVAMPS-1 to 3. While PVA and AMPS exhibited glass transition

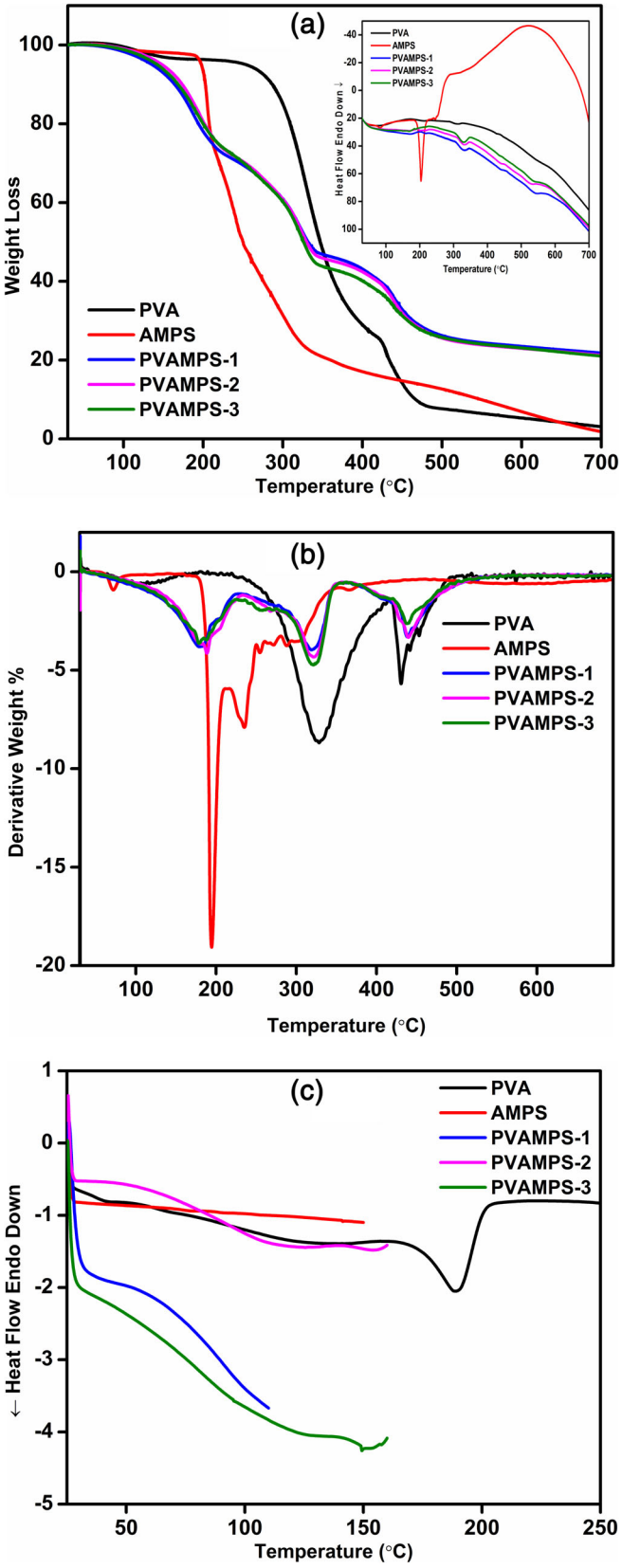

FIGURE 11 Legend on next page.

temperatures (T_g) around 116°C and 75°C, respectively, all hydrogels showed a distinct endothermic peak between 110°C and 115°C. This suggests similar material contributions despite the closely spaced T_g values. Interestingly, PVAMPS-3, with potentially less amorphous PVA due to its lower PVA content, displayed the highest T_g at 115°C. Conversely, PVAMPS-1, likely containing more PVA, had the lowest T_g at 110°C. The abundant hydrophilic hydroxyl groups in PVAMPS hydrogels, indicated by the previous TGA analysis, likely contribute to interpenetration of poly AMPS in cross-linked poly (vinyl alcohol) network and intramolecular hydrogen bonding. The observed endothermic transitions followed the order PVAMPS-1 < PVAMPS-2 < PVAMPS-3, implying increasing compactness and rigidity in the respective hydrogels. Crucially, the DSC analysis confirmed the absence of any T_g within the human body temperature range. This assures the safety of these hydrogels for wastewater treatment applications, as they would not melt or release harmful substances when in contact with human skin.[73]

3.6 | XRD study

This study focuses on the impact of PVA ratio on the crystallinity of AMPS-based hydrogels (Figure 9). The six sharp peaks at 11°, 15°, 20°, 23°, 27°, and 35° in the XRD plot of pure AMPS confirm its crystalline nature (Figure 12). In contrast, the presence of two broad peaks at 20° and 41° in the XRD pattern of pure PVA reveals its amorphous character.[51] Figure 9 further shows the XRD patterns of PVAMPS hydrogels. Interestingly, the intensity of the crystalline peaks attributed to AMPS decreases upon its incorporation into the hydrogel matrix with PVA. This suggests the formation of an amorphous phase within the PVAMPS hydrogels.

3.7 | Swelling property

The swelling behavior of PVAMPS hydrogels is observed by the Donnan equilibrium, which depends on the difference in ion concentration between the hydrogel and its surrounding environment. This concentration gradient creates an osmotic pressure, causing the hydrogel to swell or de-swell. When charged groups within the hydrogel ionize and repel each other, they drive swelling, while pH-sensitive characteristic makes PVAMPS hydrogels ideal for dye absorption applications. Figure 4 illustrates the pH-dependent swelling behavior of PVA and AMPS hydrogels at room temperature. Figure 13a–c shows the time-dependent swelling capacity of PVAMPS hydrogels. Interestingly, at pH 7.0, all PVAMPS hydrogels exhibit the highest swelling capacity, while the lowest occurs at pH 9.0. Among the tested pH values (4, 7, and 9), PVAMPS-1 displays the greatest swelling capacity, while PVAMPS-3 shows the least.

The swelling behavior of PVAMPS hydrogels depends on the pH of the solution. At neutral pH 7, the interaction between hydrophilic groups (-SO_3H) with water molecules leads to an increase in osmotic pressure within the hydrogel matrix, resulting in enhanced diffusion.

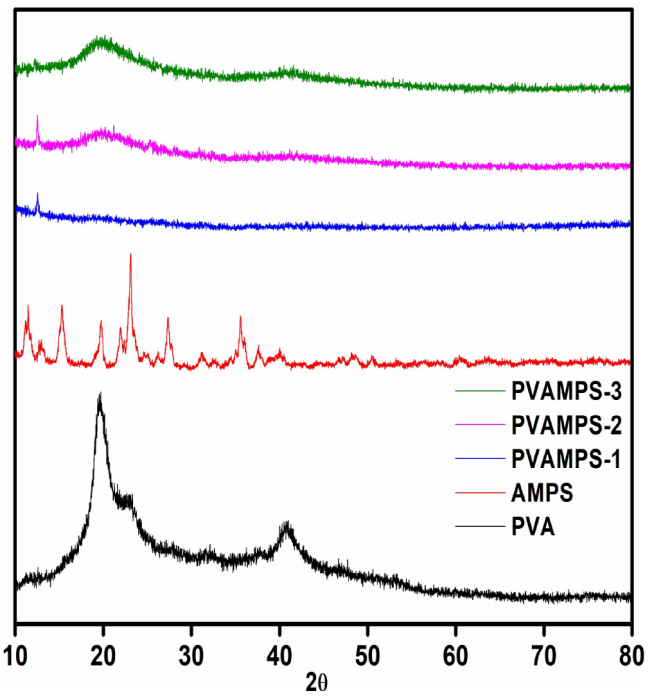

FIGURE 12 Observation of Crystallinity/Amorphous behavior of Poly (vinyl alcohol), Allylthiourea, PVAMPS-1 (1.25×10^{-4} mol/L of poly (vinyl alcohol) and 2.41 mol/L of AMPS), PVAMPS-2 (0.62×10^{-4} mol/L of poly (vinyl alcohol) and 3.62 mol/L of AMPS) and PVAMPS-3 (0.31×10^{-4} mol/L of poly (vinyl alcohol) and 4.82 mol/L of AMPS). [Color figure can be viewed at wileyonlinelibrary.com]

FIGURE 11 In this plot effect of temperature on derivative weight loss, % residual mass, DTA and DSC of PVA, AMPS, PVAMPS-1 (1.25×10^{-4} mol/L of poly (vinyl alcohol) and 2.41 mol/L of AMPS), PVAMPS-2 (0.62×10^{-4} mol/L of poly (vinyl alcohol) and 3.62 mol/L of AMPS) and PVAMPS-3 (0.31×10^{-4} mol/L of poly (vinyl alcohol) and 4.82 mol/L of AMPS) is mentioned (dried form), (a) with this plot we observed the derivative weight loss of sample with respect of temperature (DTG) (b) from this plot effect of temperature on % residual mass of samples is analyzed (TGA) (c) the effect of temperature on phase change of sample is observed with the help of this plot (DSC). [Color figure can be viewed at wileyonlinelibrary.com]

However, at acidic pH 4 and basic pH 9, the swelling capacity of the hydrogel is reduced, this is due to the protonation of the hydrophilic groups at low pH and the rapid increase in the concentration of mobile cations in the solution at high pH, respectively. The maximum swelling capacity is observed at pH 7 for both PVAMPS-1 and PVAMPS-2. However, the minimum swelling capacity is obtained at different pH values for the PVAMPS hydrogels. PVAMPS-3 has the lowest swelling capacity at pH 4, 7 and 9. This suggests that the cross-linked network and interpenetration effect of poly AMPS in the hydrogel plays a role in determining the swelling behavior at different pH values. Overall, the PVAMPS hydrogels exhibit a porous behavior, which is confirmed by the experiment over time at pH 4, 7, and 9. This makes them potential candidates for various applications, such as drug delivery and tissue engineering.

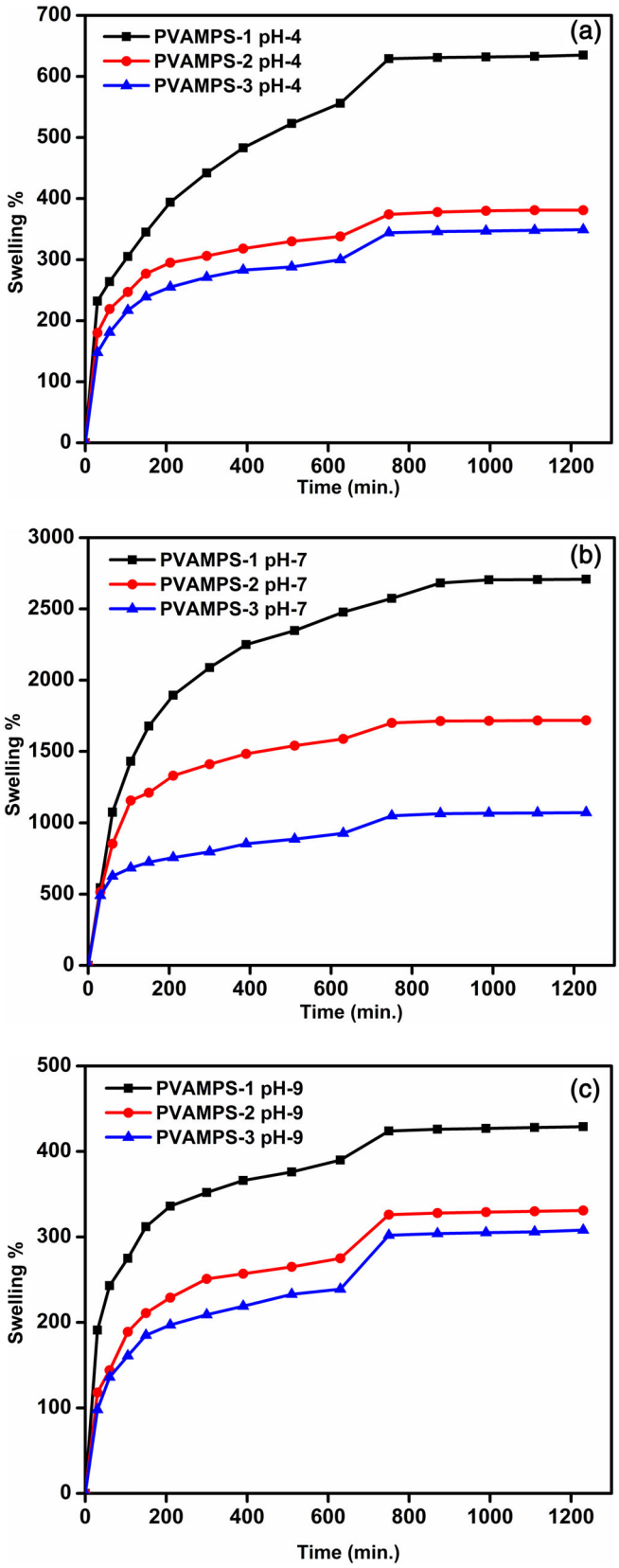

FIGURE 13 Water holding behavior of PVAMPS-1 (1.25×10^{-4} mol/L of poly (vinyl alcohol) and 2.41 mol/L of AMPS), PVAMPS-2 (0.62×10^{-4} mol/L of poly (vinyl alcohol) and 3.62 mol/L of AMPS) and PVAMPS-3 (0.31×10^{-4} mol/L of poly (vinyl alcohol) and 4.82 mol/L of AMPS) hydrogels at different pH 4, 7 and 9. [Color figure can be viewed at wileyonlinelibrary.com]

3.8 | BET surface area and porosity analysis

The PVAMPS hydrogels were assessed for their surface area and pore diameter, with results depicted in Figure 14 and summarized in Table 1. The pore size distribution, derived from nitrogen adsorption data using BJH calculations, is also illustrated in Figure 14.

PVAMPS-3 exhibited a notable BET surface area of 13.206 $m^2 g^{-1}$, accompanied by an average pore diameter of 18.0815 Å.[76] Meanwhile, PVAMPS-2 and PVAMPS-1 displayed BET surface areas of 11.033 $m^2 g^{-1}$ and 8.618 $m^2 g^{-1}$, with average pore diameters of 18.0635 Å and 18.0625 Å, respectively (Table 2). All PVAMPS hydrogels demonstrated a type IV adsorption pattern indicating a mesoporous structure with robust adsorbent-adsorbate interaction.[77] The higher surface area of PVAMPS-3 compared to PVAMPS-2 and PVAMPS-1 can be attributed to the greater number of AMPS in its hydrogel composition. Consequently, PVAMPS-3 exhibited enhanced dye adsorption capacity, with removal rates of 96%, 86%, and 94% for MB, SF, and TH, respectively. In contrast, PVAMPS-1 and PVAMPS-2 displayed slightly lower removal rates, with PVAMPS-1 at 91%, 70%, and 85% for MB, SF, and TH, and PVAMPS-2 at 94%, 78%, and 92%, respectively.

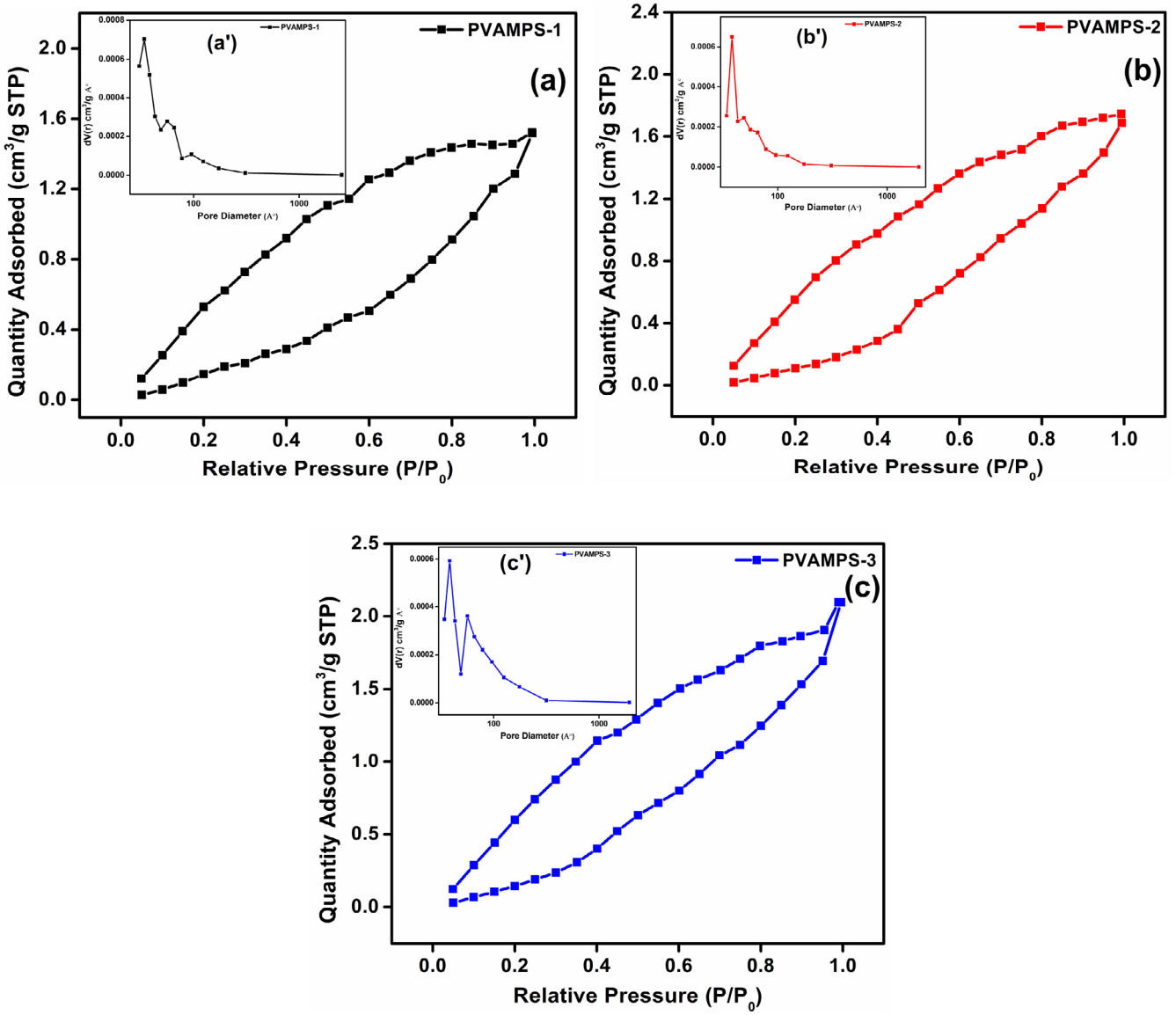

FIGURE 14 BET Surface area analysis and Pore Diameter of PVAMPS-1 (1.25×10^{-4} mol/L of poly (vinyl alcohol) and 2.41 mol/L of AMPS), PVAMPS-2 (0.62×10^{-4} mol/L of poly (vinyl alcohol) and 3.62 mol/L of AMPS) and PVAMPS-3 (0.31×10^{-4} mol/L of poly (vinyl alcohol) and 4.82 mol/L of AMPS) hydrogels. [Color figure can be viewed at wileyonlinelibrary.com]

3.9 | Study on adsorption of three different dyes

The dye concentration was determined by measuring the maximum UV–visible absorbance ($\lambda_{max} = 520$ nm for SF, $\lambda_{max} = 600$ nm for TH, and $\lambda_{max} = 665$ nm for MB) in PVAMPS hydrogels (Figure 15). The calibration curve, obtained according to the Beer–Lambert law, is depicted in Figures S1–S9. Contact times ranged from 60 to 21,600 min, showing an increase in adsorption capacity with prolonged contact. Three different dyes were utilized with variations of poly (vinyl alcohol) and AMPS ratio, as detailed in Table 1. Comparing PVAMPS-1 and PVAMPS-3, the latter exhibited higher adsorption capacity for all cationic dyes due to the presence of more negatively charged species facilitating stronger electrostatic interactions with the positively charged moiety of cationic dye molecules. Increasing dye concentration corresponded to higher adsorption percentages over time, peaking between 120 to 180 min (47%–80% for MB, 22%–62% for SF, and 33%–64% for TH). This observation underscores certain dyes affinity towards binding with PVAMPS hydrogels, attributed to numerous active sites on the hydrogel surface readily engaging with dye molecules upon immersion. Initially, adsorption was rapid (within 180 min), gradually slowing down thereafter (180–1440 min) as the dye concentration in the solution decreased and the solid–liquid phase gradient

TABLE 2 Details of the surface area and pore properties by BET of PVAMPS-1, PVAMPS-2 and PVAMPS-3.

Sample	BET surface area (m^2/g)	Pore volume (cm^3/g)	Average pore size (Å)
PVAMPS-1	8.618	0.009	18.0625
PVAMPS-2	11.033	0.015	18.0635
PVAMPS-3	13.206	0.017	18.0815

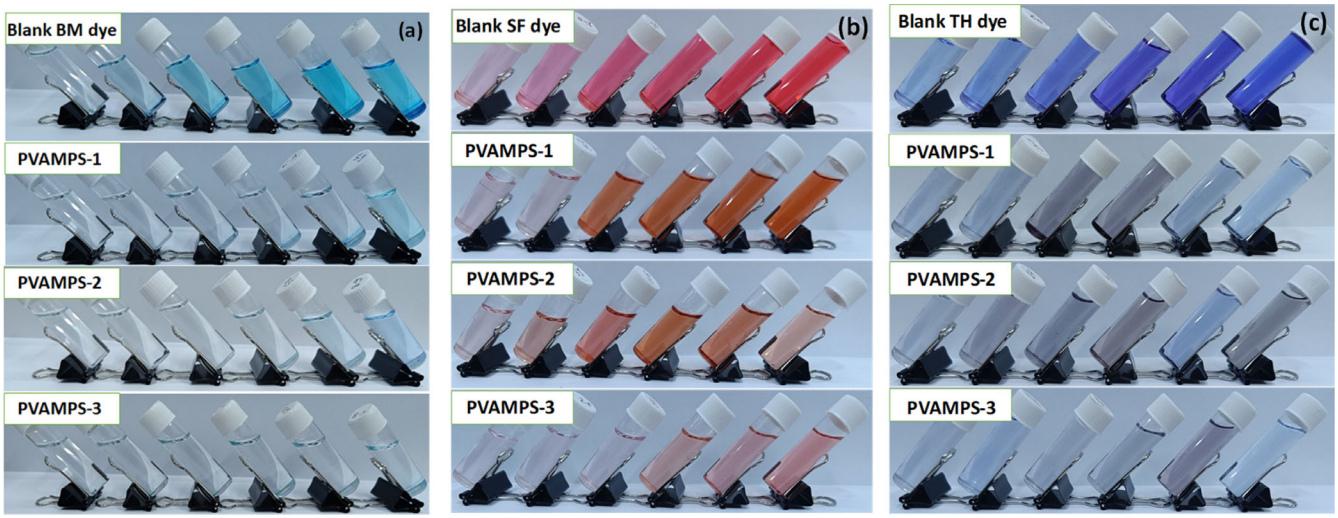

FIGURE 15 This images shows the effect on color of dye solution after adsorption with Synthesized PVAMPS hydrogels (PVAMPS-1 (1.25×10^{-4} mol/L of poly (vinyl alcohol) and 2.41 mol/L of AMPS)), PVAMPS-2 (0.62×10^{-4} mol/L of poly (vinyl alcohol) and 3.62 mol/L of AMPS) and PVAMPS-3 (0.31×10^{-4} mol/L of poly (vinyl alcohol) and 4.82 mol/L of AMPS), (a) changes in appearance of MB dye after adsorption by PVAMPS hydrogels, (b) changes in appearance of SF dye after adsorption by PVAMPS hydrogels, (c) changes in appearance of TH dye after adsorption by PVAMPS hydrogels. [Color figure can be viewed at wileyonlinelibrary.com]

diminished. Additionally, surface adsorption sites became saturated, leading to repulsive forces between dye molecules. Equilibrium was reached after 1440 min, with removal efficiencies stabilizing (96.7%, 86%, and 94% for MB, SF, and TH respectively, in PVAMPS-3 hydrogel). Equilibrium adsorption capacity was attained when all available surface sites were occupied. While PVAMPS-1 and PVAMPS-2 exhibited similar adsorption behaviors, their equilibrium removal rates varied: PVAMPS-1 showed rates of 91%, 70%, and 85% for MB, SF, and TH respectively, while PVAMPS-2 displayed rates of 94%, 78%, and 92% for MB, SF, and TH respectively (Figure S15).

3.9.1 | Adsorption kinetics

Adsorption kinetics encompasses the theoretical examination of the correlation between adsorption capacity and time during the adsorption process, as well as the investigation into adsorption rate and mechanism. Various models for adsorption rates can be formulated based on different assumptions, each applicable to different stages of speed control in the adsorption process. To study dye adsorption behavior, experimental data was fitted using both the pseudo first order (PFO) and pseudo second order (PSO) models (Figures S13 and S14) PFO fitting involved plotting adsorption time against the logarithm of the parameter log ($Q_e - Q_t$), while PSO fitting involved plotting adsorption time against the parameter t/Q_t. Figures S13 and S14 illustrates the fitting curves for both the PFO and PSO kinetic models. The resulting kinetic parameters and correlation coefficients (R^2) are presented in Tables S3–S6 for reference.

For instance, the *R*-squared (R^2) values for MB with the PFO kinetic model range between 0.93294 to 0.97528 for PVAMPS-1, 0.80836 to 0.97950 for PVAMPS-2, and 0.98562 to 0.97255 for PVAMPS-3. Similarly, the R^2 values for SF with the same model are between 0.87330 to 0.99475 for PVAMPS-1, 0.89458 to 0.98494 for PVAMPS-2, and 0.79112 to 0.96151 for PVAMPS-3. Additionally, the R^2 values for TH with the PFO kinetic model fall between 0.98869 to 0.95732 for PVAMPS-1, 0.97803 to 0.99334 for PVAMPS-2, and 0.91426 to 0.99030 for PVAMPS-3. Conversely, the R^2 value for the PSO kinetic model remains constant at 0.999 across all three dyes for

all hydrogels. Notably, the adsorption capacity calculated from the PFO kinetic fitting curve notably diverges from the PSO kinetic fitting curves. This discrepancy underscores the closer alignment of the experimental values with those presented in the Tables S3–S6. Overall, the R^2 values and the fitting of adsorption capacity strongly indicate superior fitting of the experimental data by the PSO kinetic model for all three dyes.

To investigate the adsorption mechanism of PVAMPS hydrogel adsorbents on MB, SF, and TH solutions, we primarily employed adsorption kinetics to characterize the adsorption rate. The equations for the pseudo-first-order and pseudo-second-order models are presented in Equations (7) and (8), respectively.[78,79]

$$\ln(Q_e - Q_t) = \ln Q_e - K_1 t \tag{7}$$

$$\frac{t}{Q_t} = \frac{1}{K_2 Q_e^2} + \frac{t}{Q_e} \tag{8}$$

where t (min) is the adsorption time, Q_e and Q_t (mg/g) are the adsorption capacity of MB at equilibrium time and time t, respectively, and K_1 (min^{-1}) and K_2

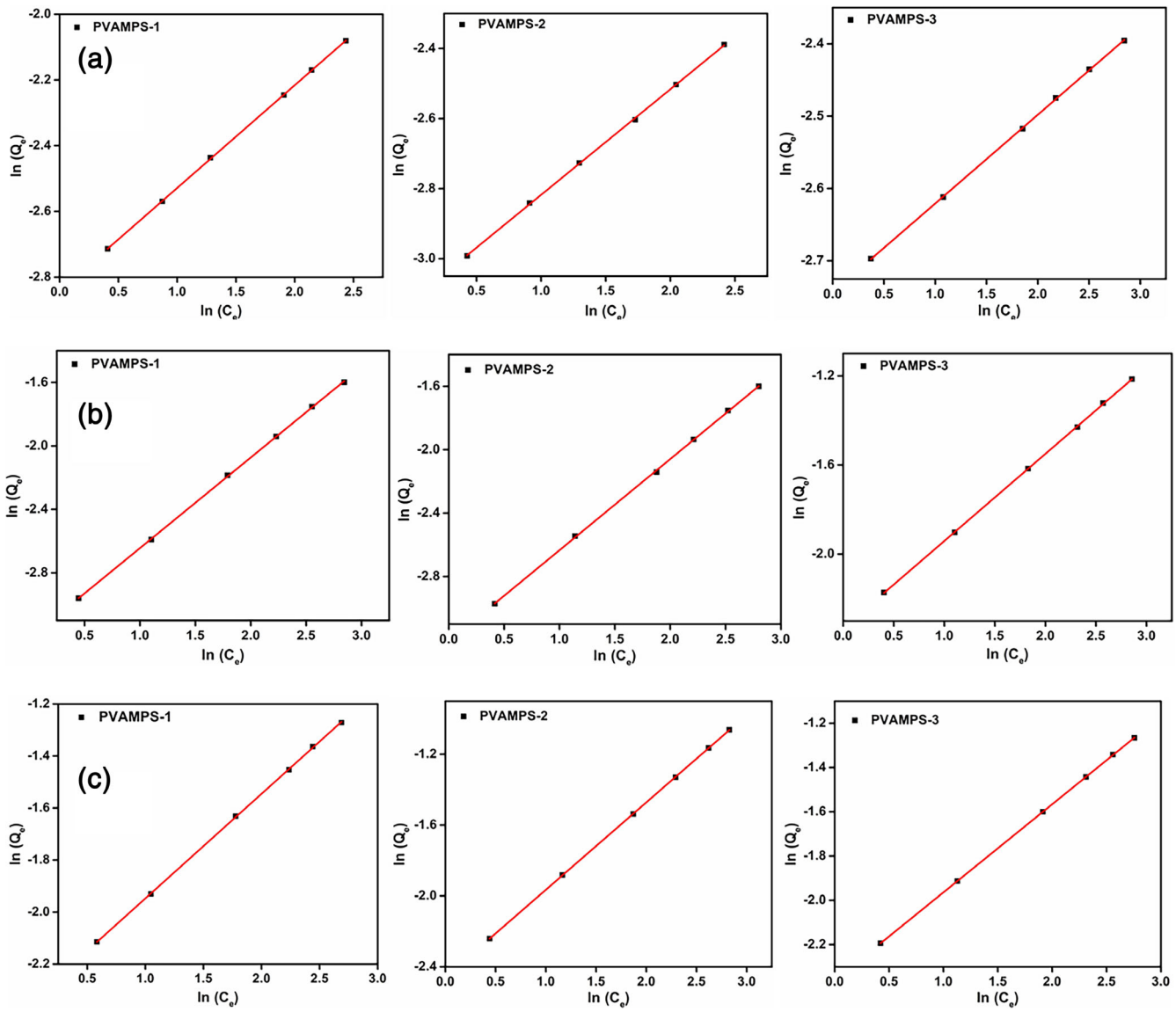

FIGURE 16 Freundlich isotherm for synthesized PVAMPS hydrogels (i.e. PVAMPS-1 (1.25×10^{-4} mol/L of poly (vinyl alcohol) and 2.41 mol/L of AMPS)), PVAMPS-2 (0.62×10^{-4} mol/L of poly (vinyl alcohol) and 3.62 mol/L of AMPS) and PVAMPS-3 (0.31×10^{-4} mol/L of poly (vinyl alcohol) and 4.82 mol/L of AMPS) at different concentrations (i.e. 5, 10, 20, 30, 40 and 50 ppm). (a) Freundlich isotherm of different concentrations of MB towards synthesized PVAMPS hydrogels, (b) Freundlich isotherm of different concentrations of SF towards synthesized PVAMPS hydrogels, (c) Freundlich isotherm of different concentrations of TH towards synthesized PVAMPS hydrogels. [Color figure can be viewed at wileyonlinelibrary.com]

($g \cdot mg^{-1}\ min^{-1}$) are the adsorption rate constants of the pseudo-first-order and pseudo-second-order equations, respectively.

3.9.2 | Adsorption isotherm

The adsorption isotherms provide insights into the interaction between the adsorbent and adsorbate, as well as the condition of the adsorbent and the structure of the adsorption layer at the interface. To explore dye adsorption behavior, both the Langmuir and Freundlich isotherm models were employed to analyze experimental data. The Langmuir model, often termed the monolayer adsorption model, assumes a uniform surface on the adsorbent with consistent adsorption capacity throughout. In contrast, the Freundlich model describes adsorption on a surface with uneven energy distribution, depicting reversible multi-molecular layer adsorption and the non-ideal process in multiphase systems. Figure 16 illustrates the impact of dye concentrations (ranging from 5 to 50 mg/L) on the adsorption capacity of the PVAMPS hydrogels. It demonstrates that with increasing dye concentration, the adsorption capacity of PVAMPS hydrogels

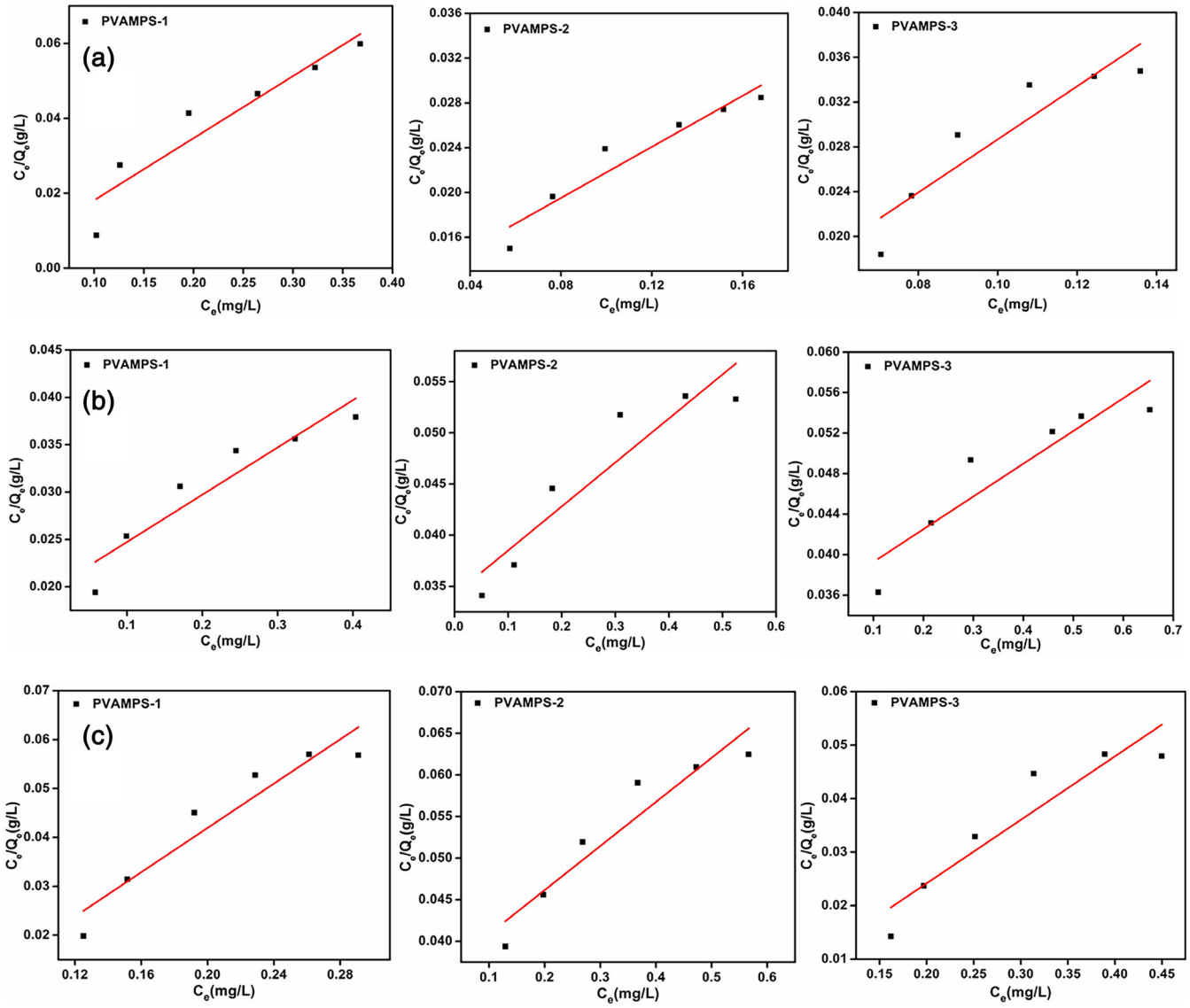

FIGURE 17 Langmuir isotherm for synthesized PVAMPS hydrogels (i.e. PVAMPS-1 (1.25×10^{-4} mol/L of poly (vinyl alcohol) and 2.41 mol/L of AMPS)), PVAMPS-2 (0.62×10^{-4} mol/L of poly (vinyl alcohol) and 3.62 mol/L of AMPS) and PVAMPS-3 (0.31×10^{-4} mol/L of poly (vinyl alcohol) and 4.82 mol/L of AMPS) at different concentrations (i.e. 5, 10, 20, 30, 40 and 50 ppm). (a) Langmuir isotherm of different concentrations of MB towards synthesized PVAMPS hydrogels, (b) Langmuir isotherm of different concentrations of SF towards synthesized PVAMPS hydrogels, (c) Langmuir isotherm of different concentrations of TH towards synthesized PVAMPS hydrogels. [Color figure can be viewed at wileyonlinelibrary.com]

rises, attributed to enhanced mass transfer driving force during adsorption. Langmuir isotherm models were generated by plotting equilibrium concentration against PVAMPS hydrogels, with C_e/Q_e as the ordinate, while Freundlich isotherm models were derived with equilibrium concentration plotted against PVAMPS hydrogels, using ln Q_e as the ordinate. Figure 17 depicts the fitting curves for the Freundlich isotherm models, and the corresponding kinetic parameters and correlation coefficients (R^2) are provided in Table S6 under the Freundlich isotherm section.

For instance, in the Langmuir isotherm model, the highest R^2 values obtained for MB, SF, and TH were 0.90271, 0.86693, and 0.88803, respectively. Conversely, in the Freundlich isotherm model, the highest R^2 values for MB, SF, and TH were notably higher at 0.99991, 0.99994, and 0.99999, respectively. This stark contrast clearly indicates that the Freundlich isotherm model provides a superior fit to the experimental data and offers a more accurate description of the adsorption mechanism. Under the specified experimental conditions, the adsorption of MB, SF, and TH dyes by PVAMPS hydrogels is characterized by heterogeneous adsorption involving multi-molecular layers. Some adsorption sites exhibit high energy and strong binding affinity towards the dyes, while others display low energy and weak interaction. Moreover, the parameter $1/\eta$ in the Freundlich model typically signifies the heterogeneity of adsorption, with smaller values indicating greater heterogeneity. Analysis of Table S3 reveals that the parameter $1/\eta$ is consistently less than 1, indicating that the hydrogel facilitates dye adsorption. Utilizing the Freundlich isotherm model to fit the isotherms for all three dyes yielded R^2 values exceeding 0.9999, with $1/n$ values hovering around 0.5. These findings underscore the spontaneous and feasible nature of the adsorption behavior.

After characterizing the adsorption kinetics, we proceeded to examine the equilibrium curves through application of the Freundlich adsorption isotherm. This model was employed to describe multilayer adsorption on the heterogeneous surface and was expressed as follows.[80]

$$\ln Q_e = \ln K_F + \frac{1}{n} \ln C_e \quad (9)$$

where K_L is the rate constant, C_e (mg/L) is the equilibrium concentration of the solution, Q_e (mg/g) and Q_{max} (mg/g) are the equilibrium and maximal adsorption amount, respectively.

$$\frac{C_e}{Q_e} = \frac{1}{Q_{max} K_L} + \frac{C_e}{Q_{max}} \quad (10)$$

K_F is the rate constant, Q_e (mg/g) represents the equilibrium adsorption amount, C_e (mg/L) stands for the equilibrium concentration of the solution, and $1/\eta$ signifies the adsorption intensity. Utilizing Equations (9) and (10), the maximum adsorption capacity (Q_{max}), the constants K_L and K_F, along with the correlation coefficients $R_L{}^2$ and $R_F{}^2$, were computed and detailed in Table S6. The findings indicate that the correlation coefficients derived from the Freundlich adsorption isotherm exceeded 0.999 in most cases, suggesting that the Freundlich adsorption isotherm proved to be more appropriate for the adsorption process of MB, SF, and TH onto PVAMPS hydrogels.

3.9.3 | Reusability test of dye adsorption

After concluding the adsorption experiment, the PVAMPS hydrogels loaded with dye were retrieved, subjected to multiple cycles of sonication and centrifugation in basic solution and distilled water, respectively, to ensure thorough removal of the dye. The dried PVAMPS hydrogels were then reused for further dye adsorption to assess their recyclability (Figure 18). Following each adsorption cycle, UV–Vis spectra of the remaining dye residues were measured (Figures S10–S12), and their maximum molar absorbances were recorded to determine both the concentration of the residual dye and the dye removal efficiency of the PVAMPS hydrogels. In this cycle we observed that the reusability ability of methylene blue dye is better, that is, beyond 90% adsorption

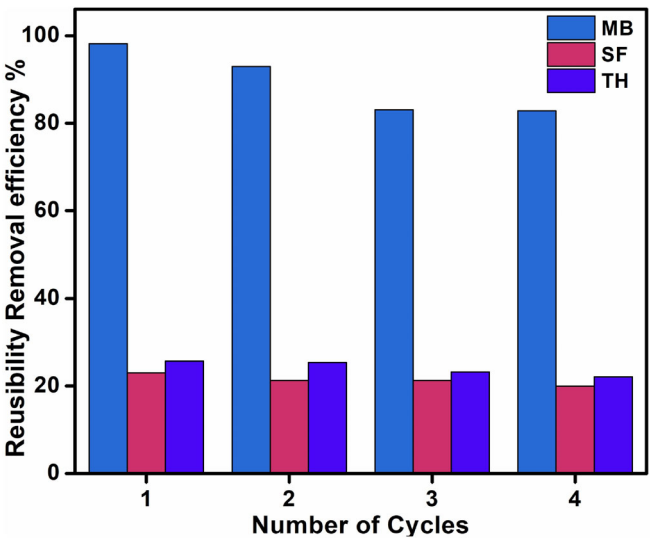

FIGURE 18 Synthesized PVAMPS hydrogels (PVAMPS-3 (0.31×10^{-4} mol/L of poly (vinyl alcohol) and 4.82 mol/L of AMPS)) reusability graph for dyes (i.e. MB, SF and TH) at 50 ppm concentration. [Color figure can be viewed at wileyonlinelibrary.com]

ability but in case of Safranine-O and thionine the adsorption of capacity in decreases, that is, 20% and 23%, respectively.

4 | CONCLUSION

In summary, PVAMPS hydrogels were successfully synthesized by cross-linking Poly (vinyl alcohol) with AMPS using glutaraldehyde, resulting a soft gel-like substrate known as PVAMPS hydrogel. The mesoporous structure of PVAMPS hydrogels was achieved through polymerization and lyophilization, resulting in favorable mechanical properties and porous nature. PVAMPS hydrogels exhibited outstanding adsorption capabilities for MB, SF, and TH dyes, with the PVAMPS-3 variant reaching equilibrium adsorption capacities of 97%, 86%, and 94% for the respective dyes, under controlled reaction conditions. The adsorption kinetics followed a PSO kinetic model, while the Freundlich isotherm model provided a better fit for the experimental data, suggesting heterogeneous adsorption of multimolecular layers. Interesting reusability of the hydrogel is observed. These promising results establish PVAMPS hydrogels as viable options for practical applications in the dyeing industry and wastewater treatment. Their thermal stability, self-healing properties, porosity, reusability and mechanical strength make them ideal candidates for addressing dye wastewater discharge.

AUTHOR CONTRIBUTIONS

Paramjeet Yadav: Conceptualization (lead); investigation (lead); methodology (lead); writing – original draft (lead). **Shere Afgan:** Methodology (lead); validation (lead); visualization (lead). **Shiwani Singh:** Data curation (equal); formal analysis (equal); software (equal); visualization (equal). **Ravi Prakash:** Investigation (equal); resources (equal). **Pralay Maity:** Data curation (equal); validation (equal). **Rajesh Kumar:** Conceptualization (lead); supervision (lead); writing – review and editing (lead).

ACKNOWLEDGMENTS

Instrumental facilities at BHU and IIT BHU Varanasi for Rheology studies are gratefully acknowledged.

FUNDING INFORMATION

Financial support from IoE Banaras Hindu University, India (Scheme No.: 6031 Incentive grant) is acknowledged by Rajesh Kumar. PY thanks CSIR-UGC-India for the NET-JRF-SRF fellowship.

CONFLICT OF INTEREST STATEMENT

There are no conflicts to declare.

DATA AVAILABILITY STATEMENT

The data that support the findings of this study are available in the Supporting Information of this article.

ORCID

Rajesh Kumar https://orcid.org/0000-0002-4243-0477

REFERENCES

[1] H. Kolya, C. W. Kang, *Toxics* **2024**, *12*, 111.
[2] F. Carolin C, T. Kamalesh, P. S. Kumar, G. Rangasamy, *Ind. Eng. Chem. Res.* **2023**, *62*, 8575.
[3] B. Cantoni, J. Ianes, B. Bertolo, S. Ziccardi, F. Maffini, M. Antonelli, *J. Environ. Manage.* **2024**, *350*, 119537.
[4] M. R. Gadekar, M. M. Ahammed, *Desalin. Water Treat.* **2016**, *57*, 26392.
[5] M. M. Bello, A. A. A. Raman, *Environ. Chem. Lett.* **2019**, *17*, 1125.
[6] M. Ahmed, M. O. Mavukkandy, A. Giwa, M. Elektorowicz, E. Katsou, O. Khelifi, V. Naddeo, S. W. Hasan, *npj Clean Water* **2022**, *5*, 12.
[7] S. L. Majamo, T. A. Amibo, D. T. Mekonnen, *Sci. Rep.* **2024**, *14*, 4540.
[8] J. Y. C. Lim, S. S. Goh, S. S. Liow, K. Xue, X. J. Loh, *J. Mater. Chem. A* **2019**, *7*, 18759.
[9] J. Li, Z. Xu, W. Wu, Y. Jing, H. Dai, G. Fang, *Colloids Surf. A* **2018**, *538*, 474.
[10] N. Ji, J. Luo, W. Zhang, J. Sun, J. Wang, C. Qin, Q. Zhuo, L. Dai, *Macromol. Mater. Eng.* **2023**, *308*, 2200525.
[11] L. Rahman, J. Goswami, *J. Package Technol. Res.* **2023**, *7*, 1.
[12] A. Liu, L. Medina, L. A. Berglund, *ACS Appl. Mater. Interfaces* **2017**, *9*, 6453.
[13] L. Yang, C. Wang, L. Chen, X. Wang, P. Cui, T. Zhang, *Fiber Polym.* **2017**, *18*, 33.
[14] W. C. Hsieh, J. J. Liau, *Carbohydr. Polym.* **2013**, *98*, 574.
[15] J. Kundu, L. A. Poole-Warren, P. Martens, S. C. Kundu, *Acta Biomater.* **2012**, *8*, 1720.
[16] K. S. Vasanthan, A. Subramaniam, U. M. Krishnan, S. Sethuraman, *J. Mater. Sci. Mater. Med.* **2015**, *26*, 20.
[17] H. Li, C. Wu, X. Yu, W. Zhang, *J. Mater. Res. Technol.* **2023**, *24*, 2279.
[18] T.-C. Ho, C.-C. Chang, H.-P. Chan, T.-W. Chung, C.-W. Shu, K.-P. Chuang, T.-H. Duh, M.-H. Yang, Y.-C. Tyan, *Molecules* **2022**, *27*, 2902.
[19] N. H. Thang, T. B. Chien, D. X. Cuong, *Gels* **2023**, *9*, 523.
[20] Y. Chen, J. Li, J. Lu, M. Ding, Y. Chen, *Polym. Test.* **2022**, *108*, 107516.
[21] A. V. Torres-Figueroa, S. Santos-Villalobos, D. E. Rodríguez-Félix, S. F. Moreno-Salazar, C. J. Pérez-Martínez, L. H. Chan-Chan, A. Ochoa-Meza, T. D. Castillo-Castro, *ACS Omega* **2023**, *8*, 44784.
[22] C. Li, M. She, X. She, J. Dai, L. Kong, *J. Appl. Polym. Sci.* **2014**, *131*, 39872.
[23] J. Yu, Y. Pan, Q. Lu, W. Yang, J. Gao, Y. Li, *Plasma Chem. Plasma Process.* **2013**, *33*, 219.
[24] M. Gorji, A. Sadeghianmaryan, H. Rajabinejad, S. Nasherolahkam, X. Chen, *J. Funct. Biomater.* **2019**, *10*, 23.
[25] R. M. Gohari, M. Safarnia, A. D. Koohi, M. B. Salehi, *Chem. Eng. Res. Des.* **2022**, *188*, 714.

[26] A. Rungrod, A. Kapanya, W. Punyodom, R. Molloy, J. Meerak, R. Somsunan, *Biomacromolecules* **2021**, *22*, 3839.
[27] O. O. Bakare, A. Gokul, A. O. Fadaka, R. Wu, L.-A. Niekerk, A. M. Barker, M. Keyster, A. Klein, *Molecules* **2022**, *27*, 3703.
[28] M. J. Ansari, R. R. Rajendran, S. Mohanto, U. Agarwal, K. Panda, K. Dhotre, R. Manne, A. Deepak, A. Zafar, M. Yasir, S. Pramanik, *Gels* **2022**, *8*, 454.
[29] C. W. Tu, F. C. Tsai, J. K. Chen, H. P. Wang, R. H. Lee, J. Zhang, T. Chen, C. C. Wang, C. F. Huang, *Polymers (Basel)* **2020**, *12*, 2835.
[30] B. Sekizkardes, E. Su, O. Okay, *ACS Appl. Polym. Mater.* **2023**, *5*, 2043.
[31] Y. Hou, S. Ma, J. Hao, C. Lin, J. Zhao, X. Sui, *Polymer* **2022**, *14*, 4037.
[32] A. Michalicha, A. Belcarz, D. A. Giannakoudakis, M. Staniszewska, M. Barczak, *Materials* **2024**, *17*, 278.
[33] M. M. Hamed, I. M. Ahmed, S. S. Metwally, *J. Ind. Eng. Chem.* **2014**, *20*, 2370.
[34] A. Milani, A. M. Ciammella, C. Degen, M. Siciliano, L. Rossi, *J. Hepatol.* **1992**, *16*, 369.
[35] D. K. Mahmoud, M. A. M. Salleh, W. A. W. A. Karim, A. Idris, Z. Z. Abidin, *Chem. Eng. J.* **2012**, *181*, 449.
[36] M. Rafatullah, O. Sulaiman, R. Hashim, A. Ahmad, *J. Hazard. Mater.* **2010**, *177*, 70.
[37] V. M. Vučurović, R. N. Razmovski, M. N. Tekić, *J. Taiwan Inst. Chem. Eng.* **2012**, *43*, 108.
[38] M. A. Ahmad, N. K. Rahman, *Chem. Eng. J.* **2011**, *170*, 154.
[39] E. Errais, J. Duplay, F. Darragi, I. M'Rabet, A. Aubert, F. Huber, G. Morvan, *Desalination* **2011**, *275*, 74.
[40] S. M. S. Danesh, H. Faghihian, S. Shariati, *Siliconindia* **2019**, *11*, 1817.
[41] K. V. Kumar, *J. Hazard. Mater.* **2007**, *142*, 564.
[42] R. W. Sabnis, *Handbook of Biological Dyes and Stains: Synthesis and Industrial Applications*, John Wiley & Sons, Inc, Hoboken, NJ **2010**. https://doi.org/10.1002/9780470586242
[43] L. Rejniak, H. Piotrowska, *Nature* **1966**, *209*, 517.
[44] P. Paul, S. G. Kumar, *J. Fluoresc.* **2012**, *22*, 71.
[45] G. R. Mahdavinia, A. Massoudi, A. Baghban, E. Shokri, *J. Environ. Chem.Eng.* **2014**, *2*, 1578.
[46] Z. Cheng, J. Liao, B. He, F. Zhang, F. Zhang, X. Huang, L. Zhou, *ACS Sustainable Chem. Eng.* **2015**, *3*, 1677.
[47] S. Chen, D. Guzman, M. R. Tsou, C. H. M. Li, M.-C. Suen, C. Gao, C.-Y. Tsou, *Polym. J.* **2023**, *55*, 45.
[48] K.-Y. Zhang, D. Li, Y. Wang, L.-J. Wang, *Int. J. Biol. Macromol.* **2023**, *253*, 126897.
[49] F. Li, G. Miao, Z. Gao, T. Xu, X. Zhu, X. Miao, Y. Song, G. Ren, X. Li, *Cellulose* **2022**, *29*, 4427.
[50] A. M. Omer, W. A.-A. Sadik, A. M. El-Demerdash, T. M. Tamer, R. E. Khalifa, M. S. Mohyeldin, N. A. Abdelwahed, *Polym. Bull.* **2021**, *78*, 6649.
[51] P. Yadav, S. Afgan, K. Pal, S. Jaiswal, P. Goswami, R. Prakash, R. Kumar, B. Koch, P. Maiti, *J. Polym. Sci.* **2024**, *62*, 3073.
[52] A. Das, E. L. Gilmer, S. Biria, M. J. Bortner, *Appl. Polym. Mater.* **2021**, *3*, 1218.
[53] H. Xie, M. A. Ayoubi, W. Lu, J. Wang, J. Huang, W. Wang, *Sci. Rep.* **2017**, *7*, 8459.
[54] P. H. S. Santos, M. A. Carignano, O. Campanella, *Gels* **2017**, *3*, 45.
[55] Y. Liu, K. Gordeyeva, L. Bergström, *Cellulose* **2017**, *24*, 1815.
[56] M. M. Rahman, J. A. Foisal, H. Ihara, M. Takafuji, *New J. Chem.* **2021**, *45*, 20107.
[57] X. Sheng, S. Li, Y. Zhao, D. Zhai, L. Zhang, X. Lu, *Polymer* **2019**, *11*, 1964.
[58] U. Gulyuz, M. Arslan, *Water Air Soil Pollut.* **2021**, *232*, 506.
[59] R. Rosa, A. Finizia, D. R. Claudio, L. Françoise, *Macromolecules* **2004**, *37*, 1921.
[60] P. Yadav, S. Afgan, V. Singh, K. Pal, S. Jaiswal, R. Kumar, B. Koch, *New J. Chem.* **2023**, *47*, 14684.
[61] S. Afgan, K. Pal, A. Srivastava, K. Nandy, P. Yadav, S. Jaiswal, R. Singh, R. K. Singh, R. Kumar, *Eur. Polym. J.* **2023**, *186*, 111853.
[62] S. Sharma, A. Kumar, R. Deepak, N. K. Kumar, B. K. Rana, *Int. J. Biol. Macromol.* **2018**, *116*, 37.
[63] X. Yang, T. Zhou, B. Ren, A. Hursthouse, Y. Zhang, *Sci. Rep.* **2018**, *8*, 10717.
[64] P. V. O. Toledo, O. D. Bernardinelli, E. Sabadini, D. F. S. Petri, *Carbohydr. Polym.* **2020**, *248*, 116765.
[65] Y. Wang, W. Wang, A. Wang, *Chem. Eng. J.* **2013**, *228*, 132.
[66] B. Tanhaei, A. Ayati, M. Lahtinen, M. Sillanpää, *Chem. Eng. J.* **2015**, *259*, 1.
[67] A. Atta, H. Ismail, H. Mohamed, Z. Mohamed, *J. Appl. Polym. Sci.* **2011**, *122*, 999.
[68] K. Kumar, B. S. Kaith, J. R. H. Mittal, *J. Appl. Polym. Sci.* **2012**, *124*, 4969.
[69] J. Qiao, T. Hamaya, T. Okada, *Polym. J.* **2005**, *46*, 10809.
[70] I. Korbag, S. M. Saleh, *Int. J. Environ. Stud.* **2016**, *73*, 226.
[71] H. K. Karlsson, H. Makhool, M. Karlsson, H. Svensson, *Sep. Purif. Technol.* **2021**, *256*, 117789.
[72] H. Hendrawan, K. Fitri, S. Yaya, D. P. Austina, IOP Conference Series: Materials Science and Engineering. **2018** 509 (13th JCC), https://doi.org/10.1088/1757-899X/509/1/012048
[73] H.-W. Gao, R.-J. Yang, J.-Y. He, L. Yang, *J. Appl. Polym. Sci.* **2010**, *116*, 1459.
[74] Y. Shi, D. Xiong, J. Li, K. Wang, N. Wang, *RSC Adv.* **2017**, *7*, 1045.
[75] F. Reguieg, L. Ricci, N. Bouyacoub, M. Belbachir, M. Bertoldo, *Polym. Bull.* **2020**, *77*, 929.
[76] Y. Deng, J. Chen, J. Huang, X. Yang, X. Zhang, S. Yuan, W. Liao, *Cellulose* **2020**, *27*, 3971.
[77] L. Heath, L. Zhu, W. Thielemans, *ChemSusChem* **2013**, *6*, 537.
[78] Y. Zheng, S. Hua, A. Wang, *Desalination* **2010**, *263*, 170.
[79] A. Mittal, J. Mittal, A. Malviya, V. K. Gupta, *J. Colloid Interface Sci.* **2010**, *344*, 497.
[80] A. Mittal, L. Kurup, J. Mittal, *J. Hazard. Mater.* **2007**, *146*, 243.

SUPPORTING INFORMATION

Additional supporting information can be found online in the Supporting Information section at the end of this article.

How to cite this article: P. Yadav, S. Afgan, S. Singh, R. Prakash, P. Maity, R. Kumar, *J. Appl. Polym. Sci.* **2025**, *142*(6), e56471. https://doi.org/10.1002/app.56471